ELSEVIER

Coordination Chemistry Reviews
215 (2001) 347–377

COORDINATION CHEMISTRY REVIEWS

www.elsevier.com/locate/ccr

The renaissance of homoatomic nine-atom polyhedra of the heavier carbon-group elements Si–Pb

Thomas F. Fässler

Eduard-Zintl-Institute, Technical University of Darmstadt, Hochschulstraße 10, D-64289 Darmstadt, Germany

Received 11 October 2000; accepted 22 November 2000

Contents

E-mail address: faessler@ac.chemie.tu-darmstadt.de (T.F. Fässler).

PII: S0010-8545(01)00321-6

Abstract

Homoatomic nine-atom clusters of the elements Si, Ge, Sn, and Pb represent a fascinating class of molecules. The Zintl anions $[E_9]^{x-}$ occur with different charges x and various shapes. Mixed valent compounds and polymeric chains via cluster linkage promise outstanding physical and chemical properties. A summary of recent progress in synthesis, crystal structure, EXAFS investigations, chemical bonding, Raman spectroscopy, mass spectrometry, and chemical reactivity is given. The shapes of about 30 Zintl ions $[E_9]$ are analysed. Finally, it is shown that a close relationship exists between the compounds with anionic nine-atom clusters of elements of the carbon group and the superconducting fulleride salts, which contain negatively charged polyhedra of the lightest element in this group.

Keywords: Nine-atom clusters; Zintl ion; Magnetic properties; Group 14 elements; EXAFS; Mass spectrometry

1. Introduction

Ligand free Group 14 atom polyhedra are molecules of captivating beauty and simplicity. They are highly reactive and can be formed by the reduction of the elements Si to Pb, they can also be obtained as well-defined compounds with homoatomic clusters of uniform size. Most common among them are nine-atom clusters $[E_9]$, which can already be regarded as small charged element particles that open new possibilities for chemical reactions and the development of nano-scaled materials [1]. Compounds and materials containing larger clusters of Si and Ge show interesting physical properties [2,3]. In contrast to the field of main-group element clusters, small particles of transition-metal elements are more widely studied [4–8]. Even then, it is still difficult to obtain the ligand-free transition element clusters of uniform cluster size, which is desirable for applications in nano-technology. Recent progress in synthesis of nine-atom clusters and reports on cluster coupling, put the basis of the idea of a controlled stepwise growth of large ligand-free main-group element clusters from $[E_9]$ species. The fact that compounds containing mixed valent clusters $[E_9]^{x-}$ ($x = 2$–4) exist makes them highly interesting candidates for building blocks in materials. The significance can be seen in the examples of the related fulleride salts A_3C_{60} (A = alkali metal). Here, the transition temperature of the formation of the superconducting phase correlates with the distance between the fulleride anions $[C_{60}]^{3-}$ [9,10].

Group 14 element clusters are stable with relatively low charges, and uncharged clusters represent novel element modifications, just as it is the case for fullerene cages and nanotubes C_n — simply clusters of the lightest Group 14 element. The elements of the carbon group themselves are especially prominent with respect to technical applications, chemical reactivity and chemical bonding. Going down the periodic table in Group 14, the transition from insulating elements to metals occurs. Under standard conditions the elements above Sn are insulators or semiconductors. Sn has the outstanding property that the semiconducting low temperature α-form and the metallic β-form are almost equal in energy. Even the energy difference of 1 kcal mol^{-1} is small, chemical bonding changes from localised two-centre–two-electron (2c–2e) bonds and coordination number four for all atoms (diamond structure) to metallic bonding with a coordination number higher than the valence of Sn. The phase transitions from α- to β-modification of Si and Ge are achieved by applying high pressures. The heaviest element Pb is a typical metal with delocalised bonds, but electrons form localised chemical bonds when Pb is alloyed with electropositive metals. The change in chemical bonding and thus the ability to form structures in which atoms have higher coordination numbers originate from the central position in the periodic table. This enables these elements to form homoatomic clusters in solid state, in solution and in gas phase.

The elements E = Si–Sn also form molecular cages with localised homoatomic bonds and several structures of cages $(ER)_n$ were determined crystallographically during the past years (Fig. 1a). Each cluster edge represents a 2c–2e bond and all

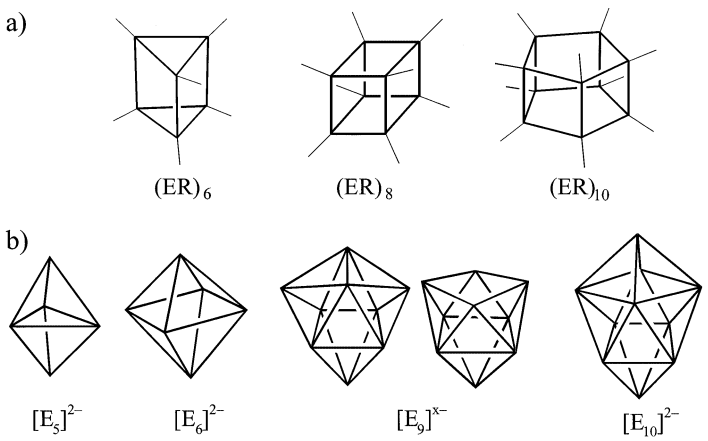

Fig. 1. (a) Structures of molecular Group 14 cages of the elements Si, Ge, and Sn [85]. Trigonal prism Ge_6 in $[(Me_3Si)_2CHGe]_6$, cubes Si_8, Ge_8, Sn_8 in $[RE]_8$, and pentagonal prism in $[RSn]_{10}$ (R = 2,6-diethylphenyl). *E*–*E* distances (in Å) in the order of the compounds: 2.56–2.58 (Ge_6), 2.38–2.45 (Si_8), 2.48–2.50 (Ge_8), 2.84–2.86 (Sn_8), 2.86 (mean value in Sn_{10}). (b) Structures of soluble homoatomic Group 14 anions $[E_5]^{2-}$, E = Ge [68], Sn, Pb [69,86]; $[E_6]^{2-}$ in $[\{E–Cr(CO)_5\}_6]^{2-}$ with E = Ge [87] Sn [88]; $[E_9]^{x-}$ (E = Si–Pb, $x = 3$, 4, Table 1), and $[Ge_{10}]^{2-}$ [14]. *E*–*E* distances (in Å) in the order of the compounds: 2.48–2.70 (Ge_5), 2.85–3.10 (Sn_5), 3.00–3.24 (Pb_5), 2.52–2.54 (Ge_6), 2.93–2.96 (Sn_6); longest intracluster distances in E_9 see h_1–h_3 in Table 1; 2.51–2.95 (Ge_{10}).

atoms of the molecules reach their octet. The homoatomic bonds are elongated by a maximum of 5%, if compared to the interatomic distances in the α modifications, mainly due to ring strains of the cages.

In the case of electron deficiency, the elements can form homoatomic multiple bonds [11], and just recently the series of compounds of the formula $R_2E{=}ER_2$ was completed with the heaviest element Pb [12,13]. Electron deficiency can alternatively be compensated by the formation of two-electrons-more-centres bonds. This requires higher coordination numbers, common for the heavier members of Group 14. In accordance with skeletal electron counting rules (see Section 4.1) naked, ligand-free deltahedral anions of the elements Si–Pb are stable candidates (Fig. 1b). $[E_9]$ and $[E_{10}]$ clusters are the largest, structurally characterised cluster anions of Group 14 elements. Only two 10-atom clusters $[Ge_{10}]^{2-}$ and $[TlSn_9]^{3-}$ are reported so far; unfortunately, both X-ray structure determinations suffer of disorder and superposition with a nine-atom cluster, respectively [14,15]. Thus the nine-atom family represents the largest family of well characterised, naked clusters.

1.1. Brief history of nine-atom clusters

The story of homoatomic clusters traces back to the observations made by Joannis in 1890, who found, that Pb dissolves in the presence of alkali metal (A) in liquid ammonia under formation of intensively coloured solutions [16]. As it was shown many years later, Joannis' solutions contained $[Pb_9]$ species. Kraus, Smyth, and Zintl [17–23] made major steps to develop the picture of polyanions of the semi-metals and metals, which were later named Zintl ions, after the famous German chemist Eduard Zintl. Since the first structure determination of a homoatomic nine-atom polyhedron in the compound $(Na^+)_4[Sn_9]^{4-}(en)_7$ (en = ethylenediamine) by Kummer et al. in 1976 [24], around 30 compounds containing homoatomic nine-atom clusters were characterised by single crystal X-ray diffraction (Table 1).

In all cases, the clusters are formed by reduction of the elements Si, Ge, Sn, and Pb with alkali metals or by electrochemical methods (Sn, Pb). The breakthrough in structural characterisation was the introduction of alkali-metal sequestering cryptand molecule (cp)[1] by Corbett [25]. Until 1997 all structurally characterised compounds were obtained by extraction of pre-formed binary phases of the approximate nominal composition A/E = 4:9 with en and subsequent crystallisation with cryptand. Electrochemical methods were used for the synthesis and the characterisation of the clusters in solution [26].

1.2. Scope

Up to this point the field of nine-atom clusters was embedded in several review articles [27–30]. Recent results put forth the knowledge and chemistry of E_9

[1] cp = [2.2.2] crypt = 4,7,13,16,21,24-hexaoxa-1,10-diazabicyclo-[8.8.8]hexacosane.

Table 1
Values of geometrical parameters for nine-atom clusters. Parameters see Fig. 4

	Compound			Prism edges[a,b]					Dihedral angles[c]					
		[d]	*el*[e]	h_1	h_2	h_3	γ[b]	h/e[f]	α_1	α_2	α_3	d_1/d_2[g]	[h]	
	$[B_9X_9]$ (X = Cl, Br)		18	1	1	1	0	1.15	20	20	20	–	**I**	[66,67]
	$(Rb^+)_2$ $[B_9H_9]^{2-}$		20	1.02	1.02	1	0	0.96	25	20	20	–	**I**	[61,89]
	(Bi^+) $[Bi_9]^{5+}$ $([HfCl_6]^{2-})_3$[i]		22	1.00	1.00	1	0	1.15	22	22	22	–	**I**	[64]
	$([Bi_9]^{5+})_2$ $([BiX_5]^{2-})_8$ $([Bi_2X_8]^{2-})_2$[i] (X = Cl, Br)		22	1.07	1.00	1	6	1.19	14	24	24	–	**III**	[65,90]
1a	$(Rb^+)_{12}([Si_4]^{4-})_2$ $[Si_9]^{4-}$[i]	**A**	22	1.26	1.08	1	16, 26	1.15, 1.08	9	25	30	1.08	**V**	[33]
		B	22	1.21	1.20	1.03	12, 38	1.19	16	17	27	1.23	**IV**	
		C	22	1.25	1.14	1.06	12, 33	1.20, 1.15	21	21	25	1.13	**V**	
		D	22	1.20	1.15	1.04	10, 35	1.16	19	20	26	1.20	**IV**	
2a	$(Cs^+)_4[Ge_9]^{4-}$[i]	**A**	22	1.27	1.00	0.99	20, 25	–	4	26	30	1.02	**II**	[31]
		B	22	1.25	1.05	0.98	18, 25	–	7	25	33	1.04	**II**	
		C	22	1.19	1.05	1.00	13, 31	1.17	11	23	27	1.12	**III**	
		D	22	1.24	1.04	0.98	17, 29	–	6	24	27	1.07	**II**	
2b	$(K^+)_4[Ge_9]^{4-}$[i,j]	**A**	22	1.27	1.00	0.97						1.03	**II**	[32]
2c	$(Rb^+)_4[Ge_9]^{4-}$ (en)[i]	**A**	22	1.26	0.98	0.98	21, 21	1.16	0	31	31	1.00	**II**	[48]
		B	22	1.19	1.05	1.03	12, 31	1.20	10	25	25	1.12	**III**	
		C	22	1.18	1.06	1.03	10, 32	1.20	10	23	25	1.14	**III**	
2d	$[K^+-(18\text{-crown-}6)]_2$ $^1_\infty[Ge_9]^{2-}$		22	1.11	0.95	0.94	12, 29	1.07	0	25	27	1.23	**III**	[36]
2e	$[K^+\text{-cp}]_3[Ge_9]^{3-}$ $(en)_{0.5}$[i]		21	1.16	1.10	1[a]	10	1.17	16	18	31	1.25	**V**	[91]
2f	$[K^+\text{-cp}]_3[Ge_9]^{3-}(PPh_3)$[i]		21	1.14	1.12	0.98	10	1.17	14	17	32	1.17	**IV**	[14]
2g	$[K^+\text{-cp}]_6[Ge_9Ge_9]^{6-}(en)_{0.5}$	**A**	21	1.12	0.99	0.97	10	1.10	5	23	24	1.25	**III**	[49]
		B	21	1.21	1.00	0.97	17, 28	1.13	3	25	27	1.12	**III**	
2h	$[K^+\text{-cp}]_6[Ge_9Ge_9]^{6-}$ $(en)_{1.5}$[i]	**A**	21	1.15	0.97	0.97	13, 18	1.11	1	26	26	1.21	**III**	[49]
		B	21	1.24	0.97	0.95	20, 22	1.12	3	28	31	1.06	**II**	
2i	$[K^+\text{-cp}]_6[Ge_9Ge_9]^{6-}(en)_{2.5}$[i]	**A**	21	1.12	0.99	0.98	9	1.11	8	23	25	1.26	**III**	[25]
		B	21	1.21	1.00	0.97	18, 24	1.21	5	24	32	1.02	**II**	
2j	$[K^+\text{-cp}]_2$ $(Cs^+)_4$ $([Ge_9]\text{–}[Ge_9])^{6-}(en)_6$[i]		22	1.19	0.97	0.97	17, 26	1.19, 1.06	1	27	28	1.12	**III**	[37]
3a	$(Rb^+)_{12}([Sn_4]^{4-})_2$ $[Sn_9]^{4-}$[i]		22	1.19	1.11	0.99	12	1.16	11	20	26	1.16	**V**	[92]
3b	$(Na^+)_4$ $[Sn_9]^{4-}(en)_7$[i]		22	1.19	1.16	0.99	13	1.19	13	16	34	1.19	**IV**	[24]
3c	$[K^+\text{-(18-}crown\text{-6)}]_4[Sn_9]^{4-}$		22	1.11	1.08	1.04	4	1.14	15	17	22	1.32	**V**	[40]
3d	$[K^+\text{-(18-}crown\text{-6)}]_3(K^+)[Sn_9]^{4-}(en)$		22	1.17	1.06	1.05	8	1.15	13	22	24	1.21	**III**	[40]

Table 1 (*Continued*)

	Compound	[d]	*el*[e]	Prism edges[a,b] h_1	h_2	h_3	γ[b]	h/e[f]	Dihedral angles[c] α_1	α_2	α_3	d_1/d_2[g]	[h]	
3e	$[Na^+\text{-cp}]_4[Sn_9]^{4-}$ [i]		22	1.32	1.04	1.01	22, 22	1.19	3	29	30	1.01	**II**	[94]
3f	$[K^+\text{-cp}]_3(K^+)[Sn_9]^{4-}$		22	1.29	1.03	1.00	20, 24	1.19	2	28	29	1.02	**II**	[95]
3g	$[K^+\text{-cp}]_3[Sn_9]^{3-}(en)_{1.5}$ [i]		21	1.04	1.04	1.02	1	1.08	17	18	18	1.45	**I**	[96]
3h	$[K^+\text{-cp}]_3[Sn_9]^{3-}(en)_{0.5}$		21	1.11	1.01	1.01	7	1.08	10	21	22	1.32	**III**	[93]
3i	$[K^+\text{-cp}]_6([Sn_9][Sn_9])^{6-}(en)_{1.5}$ $(tol)_{0.5}$	**A**	21	1.10	1.02	1	6	1.08	13	19	23	1.34	**III**	[59]
		B	21	1.17	0.99	0.98	14	1.07	7	20	31	1.20	**III**[k]	
		C	21	1.14	1.02	1.00	9	1.09	15	18	25	1.18	**III**[k]	
3j	$[K^+\text{- cp}]$ $(Cs^+)_7$ $([Sn_9]^{4-})_2$ $(en)_4$		22	1.29	1.00	1.00	22, 22	1.17	1	28	29	1.01	**II**	[97]
3k	$[K^+\text{-cp}]$ $\{(CO)_3Cr\text{-}[Sn_9]\}^{4-}$ [l]	**A**	22	1.36	0.99	0.99	27, 27	–	0	25	27	1.00	**II**	[74]
4a	$(K^+)_4$ $[Pb_9]^{4-}$	**A**	22	1.31	1.06	1.02	20, 20	–	0	32	33	1.00	**II**	[98]
		B	22	1.16	1.16	1.03	9	1.16	17	17	28	1.05	**IV**	
4b	$(Cs^+)_4$ $[Pb_9]^{4-}$ [i]		22	1.29	1.06	1.01	19, 27	–	5	23	27	1.04	**II**	[83]
4c	$[K\text{-}(18\text{-crown-}6)]_4$ $[Pb_9]^{4-}$		22	1.32	1.04	0.99	23, 23	–	0	28	30	1.00	**II**	[84]
4d	$[K^+ - cp]_3$ (K^+) $[Pb_9]^{4-}$		22	1.30	1.03	1.00	21, 21	–	1	29	31	1.01	**II**	[48]
4e	$[K^+ - cp]_3$ $[Pb_9]^{3-}$ $(en)_{1.5}$		21	1.08	1.01	1.01	4	1.08	14	20	21	1.36	**III**	[99]
4f	$[K^+ - cp]_6$ $([Pb_9][Pb_9])^{6-}$ $(en)_{1.5}$ $(tol)_{0.5}$	**A**	21	1.07	1.02	1	4	1.07	16	18	23	1.38	**III**	[59]
		B	21	1.15	0.98	0.98	12	1.05	12	30	21	1.29	**III**[k]	
		C	21	1.08	1.02	0.99	6	1.07	18	19	20	1.41	**III**[k]	
4g	$[K^+ - cp]$ $\{(CO)_3$ $Cr\text{-}[Pb_9]\}^{4-}$		22	1.34	1.00	0.98	26, 25	–	0	25	29	1.00	**II**	[74]

[a] Relative prism heights, scaled to the value Si 2.56 Å, Ge 2.87 Å, Sn 3.19 Å, and Pb 3.35 Å.
[b] The best trigonal prism is chosen. If the structure is close to C_{4v} symmetry, two choices of trigonal prisms, which are rotated by approximately 90°, are possible.
[c] Dihedral cap-to-cap fold angle α about h.
[d] **A**, **B**, **C**, **D** denote different cluster isomers E_g.
[e] Numbers of skeletal electrons.
[f] In the case of two values, the second one is calculated with only two heights.
[g] The best monocapped square antiprism is chosen. If the structure is close to D_{3h} symmetry, the longest height is considered as a diagonal in the C_{4v} symmetric cluster.
[h] Cluster type see Fig. 4 and Section 5.3.
[i] Crystal structure refinement with $R_1 > 0.08$.
[j] A second crystallographically different cluster is disordered. No further data are reported.
[k] Cluster with C_1 symmetry.
[l] There are two crystallographically different clusters with the same shape.

clusters: the proof that nine-atom anions are also present in binary alloys was produced at the same time using Raman spectroscopy and X-ray diffraction methods in 1997 [31,32] and culminated in the structural characterisation of the first $[Si_9]^{4-}$ clusters in the binary phase $Rb_{12}Si_{17}$ one year later [33,34]. The possibility that the clusters can easily be obtained by reduction of the elements Sn and Pb in molten 18-crown-6 in a one-pot synthesis and that single crystals from solutions containing $[Sn_9]^{4-}$ and $[Pb_9]^{4-}$ can also be grown using the much cheaper 18-crown-6 instead of cp [35,40], finally led to the isolation of an anionic polymer consisting of $[Ge_9]^{2-}$ [36]. The possibility of cluster linkage via oxidation was indicated just one year before by the isolation of the anionic dimer $([Ge_9]-[Ge_9])^{6-}$ [37].

The present review summarises the developments during the past years and gives an overview of the shapes of nine-atom clusters known so far.

2. Synthesis of nine-atom clusters

Thermal decompositions of AE phases (A = alkali metal; E = Si, Ge, Sn) were studied under dynamic vacuum (Knudsen cell) in a thermobalance [32,34]. In contrast to earlier experiments carried out for Si [38], alkali-metal loss occurs in steps under formation of the phases $A_{12}E_{17}$, A_4E_9, A_6E_{25}, $A_8E_{44/46}$, A_xE_{136} and finally leads to the elements. $A_{12}E_{17}$ and A_4E_9 contain nine-atom clusters. In all other phases E atoms form three-dimensional networks, which are related to zeolite and clathrate structures. Single crystals of the binary phases A_4E_9 and $A_{12}E_{17}$ (see Table 1) are formed by fusion of the stoichiometric amounts of the elements at high temperatures.

Soluble clusters are obtained by extraction of the 4:9 phases for E = Ge–Pb with liquid ammonia [21]. More common is the use of ethylenediamine as solvent [17,39]. A simple and efficient one-pot synthesis is the reduction of the elements Sn and Pb with Na or K in molten 18-crown-6 as reaction medium [40].

In the case of the conducting elements Sn and Pb, clusters are also formed by electrochemical reduction using rods of the elements as electrodes [20,23,41]. Crystalline samples of the nine-atom clusters via electrochemical methods have not been reported, but many other homo- and hetero-atomic anions were isolated using this technique [42].

3. Crystalline compounds with nine-atom clusters

Discrete $[E_9]^{4-}$ and $[E_9]^{3-}$ clusters are predominant in crystalline compounds and there are indications that clusters with 2−, 3− and 4− charges coexist in one compound [43]. Depending on the counter ions the crystalline compounds that contain nine-atom anions can be divided into four groups (see Sections 3.1 and 3.4).

3.1. Binary phases A_4E_9 and $A_{12}E_{17}$

$[E_9]^{4-}$ clusters occur in binary phases of the composition A_4E_9 and $A_{12}E_{17}$ (Table 1). The clusters are discrete, i.e. they are separated by the alkali-metal atoms and there are no intercluster bonds. Applying the Zintl–Klemm–Busmann concept [44,45], i.e. transferring the valence electron of the electropositive alkali metal to the Group 14 atoms, leads in the case of the composition A_4E_9 to $[E_9]^{4-}$ cluster anions. In $A_{12}E_{17}$ two tetrahedral cluster anions $[E_4]^{4-}$ occur per $[E_9]^{4-}$ and thus $A_{12}E_{17}$ can be rewritten as $(A_4E_4)_2(A_4E_9)$. The compounds represent typical salt-like intermetallics and using molecular orbital descriptions including electron-counting rules for polyhedra (see Section 4.1), the phases can be assigned to the class of Zintl phases. With the exception of A_4Si_9 and contrarily to $A_{12}E_{17}$ the 4:9 phases are soluble in en. The compounds can therefore be regarded as salts. X-ray structure determination of single crystals of $Rb_{12}Si_{17}$, Cs_4Ge_9, $Rb_{12}Sn_{17}$, K_4Pb_9, Cs_4Pb_9 (Table 1) show that the cluster anions are ordered. Disordered clusters or crystal twinning are observed in $A_{12}Ge_{17}$ (A = Na, K) and K_4Ge_9. Ion packing of the latter two compounds can be described as hierarchical analogues of the $MgZn_2$-type ($[(A_4E_9)_1(A_4E_4)_2]$) and the Cr_3Si-type ($[(M_4E_9)_3(M_4E_9)_1]$), respectively [32].

In binary phases up to four different clusters per unit cell, which are not related by symmetry, are realised (**A**–**D** in Table 1). The anions possess different shapes, but due to the ratio of alkali-metal cations to cluster anions, the clusters are clearly $[E_g]^{4-}$ species. In order to classify E_4 and E_9 units as discrete clusters, contacts between the atoms of different clusters should be substantially longer than intracluster atom-to-atom distances. In $Rb_{12}Si_{17}$ and $Rb_{12}Sn_{17}$ the shortest distance occurs between tetrahedral clusters. The intercluster contact of 4.6 and 4.7 Å is significantly longer than intracluster contacts, which are smaller than 3.0 and 3.77 Å for $Rb_{12}Si_{17}$ and $Rb_{12}Sn_{17}$, respectively. In Cs_4Ge_9 the shortest intercluster contact is 3.96 Å, while the longest polyhedral edge is 3.62 Å. K_4Pb_9 contains discrete units [46], but is at the border to a compound with an extended framework structure [47]. The shortest intercluster separation is observed between atoms of one kind of the two independent clusters. The distance of 3.67 Å is close to the range of intracluster contacts along the edges of the polyhedra, which are in the range of 3.08–3.54 Å (Fig. 2b). Nonetheless, K_4Pb_9 dissolves in en under formation of polyanions, which confirms that the ionic description is valid. Larger alkali-metal atoms produce larger cluster-to-cluster separations and thus the shortest intercluster distance in Cs_4Pb_9 is 3.77 Å, whereas intracluster contacts are similar to those in K_4Pb_9.

3.2. Solvates $Na_4Sn_9(en)_7$ and $Rb_4Ge_9(en)$

Polar solvents such as liquid ammonia or en are able to break up the ion packing of the neat solids of the nominal composition $AE_{2.25}$ (E = Ge, Sn, Pb) and crystalline compounds are obtainable as en adducts. In $Na_4Sn_9(en)_7$ [24] two Na atoms are coordinated to four N atoms of en molecules and are not in direct contact with the cluster. The remaining two Na atoms are located above two almost

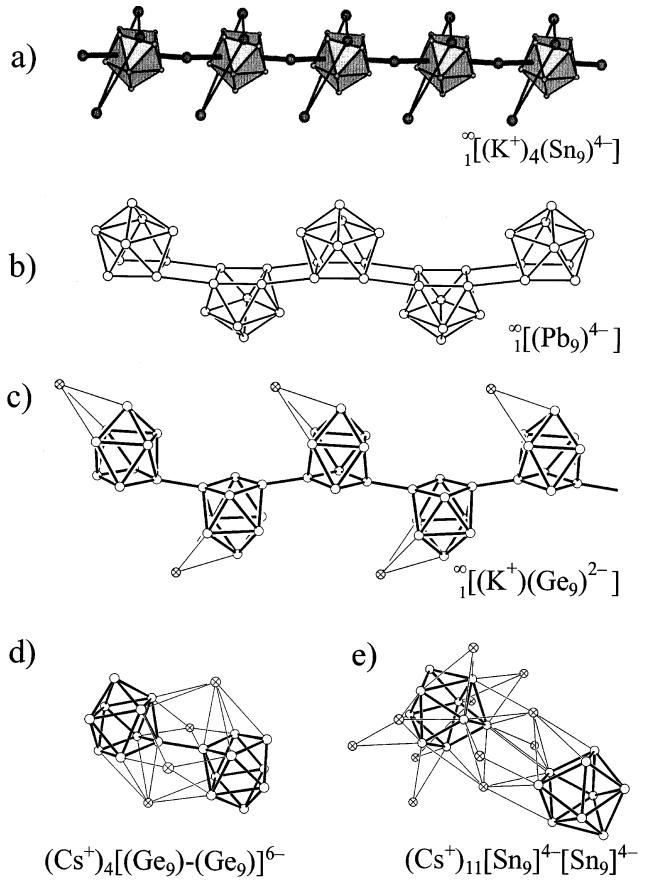

Fig. 2. Structure details of: (a) [K-(18-crown-6)]$_3$($_{\infty}^{1}$[KSn$_9$])(en) (**3d**); (b) K_4Pb_9 (**4a**); (c) [K-(18-crown-6)]$_2$ $^{1}_{\infty}$[Ge$_9$] (**2d**); (d) [K-cp]$_2$Cs$_4$ ([Ge$_9$]–[Ge$_9$])(en)$_6$ (**2j**); and (e) [K-cp]Cs$_7$ [Sn$_9$]$_2$(en)$_4$ (**3j**).

parallel edges of the cluster. Even this compound class led to the first structure determination of a nine-atom species, only one further report of a crystalline en adduct is known. In $Rb_4Ge_9(en)_{1.1}$ the $[Ge_9]^{4-}$ clusters are surrounded by 12 Rb cations, which form a cavity around the anion. There are three types of symmetry independent en molecules, which lie in octagonal channels of the three-dimensional framework of Rb_4Ge_9. They have no contact with Rb cations. All atom positions of the en molecules are partially occupied. Full occupation would lead to two en molecules per formula unit. The ion packing can be regarded as a hierarchical derivative of the Al_4YbMo_2 structure type with the formal partial atom-to-cluster replacement $Rb_4[Ge_9](en)_2$ [48]. As in neat solids, all clusters in solvate crystals are $[E_9]^{4-}$ species.

3.3. Crown ether coordinated cations $[K\text{-}(18\text{-crown-}6)]_m[E_9](en)_p$ ($E = Ge$, Sn)

For a long time the addition of sequestering cps to solutions of nine-atom clusters was the only method to obtain crystals of good quality for single crystal structure determination and which did not suffer of solvent loss [27]. Recently, it was shown that the use of 18-crown-6 also leads to single crystals with ordered clusters [40]. In the crystal structures of **3c** and **3d** K atoms form the first coordination sphere of the anions. Six O atoms of 18-crown-6 complete the coordination sphere of the K atoms. Since direct anion–cation contacts are retained these compounds can be regarded as intermediates of intermetallics and salts.

The K atoms of [K-(18-crown-6)] units are in contact with the atoms of triangular or rectangular faces of the polyhedra. Some examples are shown in Figs. 2a, 2c, 3a and 3b. The latter case bears a resemblance to the coordination of the organometallic $[Cr(CO)_3]$ fragment in compounds **3k** and **4g** (Fig. 3c).

3d consists of a linear chain of $[Sn_9]^{4-}$ which alternate with K atoms (Fig. 2a). Similar chains, which exhibit alternating clusters and K atoms, are also present in **3f** and **4d**. The other three K atoms in the latter two compounds are sequestered by

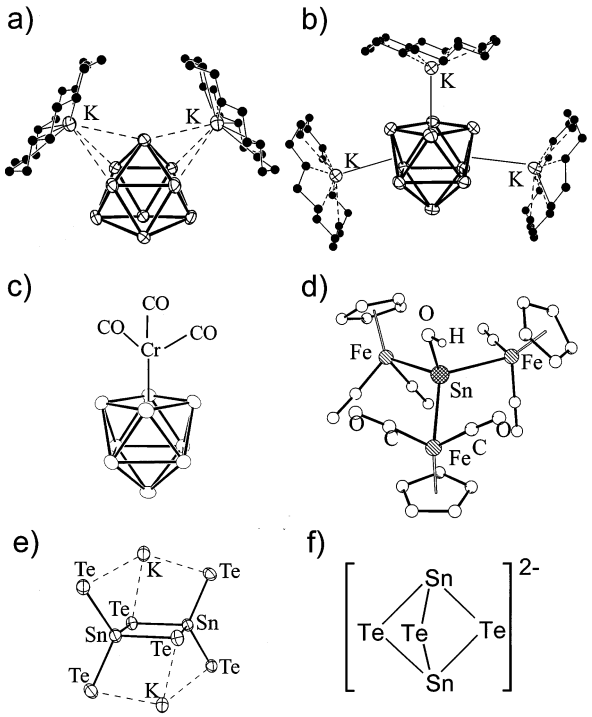

Fig. 3. Structural details of: (a) $[K\text{-}(18\text{-crown-}6)]_4[Sn_9]$ (**3c**); (b) $[K\text{-}(18\text{-crown-}6)]_4Pb_9$ (**4c**); (c) $[K\text{-}cp]_2[(CO)_3Cr]\text{-}[E_9]$) with $E = Sn$, (**3k**) and $E = Pb$ (**4g**); (d) $[Cp(CO)_2Fe]_3Sn–OH$; (e) $[K\text{-}cp]_2K_2[Te_2Sn(\mu_2\text{-}Te)_2SnTe_2](en)$; and (f) $[K\text{-}cp]_2[Sn(\mu_2\text{-}Te)_3Sn]$.

cp molecules and have therefore no contact with the cluster atoms. In **3d** each cluster is additionally coordinated to three K atoms of [K-(18-crown-6)] and the whole structure can be regarded as a composite of uncharged intermetallic chains $^{\infty}_{1}[K_4Sn_9]$, which are isolated by organic molecules. The en molecules in **3d** are not coordinated to the K atoms. Small variations of the experimental conditions during the crystallisation process decide whether **3d** or **3c** are formed. In **3c** only two [K-(18-crown-6)] units are coordinated to the anion (Fig. 3a). Layering of the en solution with toluene leads to **3d** after one week, otherwise **3c** is formed after three to four weeks.

Addition of 18-crown-6 to an en solution of K_4Ge_9 leads to a fascinating one-dimensional chain of directly connected $[Ge_9]^{2-}$ clusters (Fig. 2c). The polymer $^{1}_{\infty}[Ge_9]^{2-}$ in **2c** is built up by intercluster exo-bonds that link the basal vertices of neighbouring clusters. The intercluster contacts of 2.486(1) Å are shorter than the shortest intracluster distance of 2.522(1) Å, which can be understood by the higher degree of bond localisation in the exo-bond. The formation is a result of the oxidative coupling of $[Ge_9]^{4-}$ clusters, however, no oxidation agent has been used during the reaction. In **2c**, one type of K atoms caps a triangular cluster face. Other K atoms in **2c**, **3c**, and **4c** are coordinated to 18-crown-6 units with large distances between K and E atoms.

3.4. Cryptand-sequestered cations

3.4.1. $[A\text{-}cp]_m[E_9]$ (solvent)$_p$ ($A = Na$, K; $E = Ge$, Sn, Pb) from binary phases

The addition of cryptand to en solutions of nine-atom clusters is the most widely used method to obtain crystals of Zintl anions from solution and in the case of nine-atom polyhedra led this procedure to a large number of structurally well characterised compounds. Three types of crystals, which contain different numbers of cations and $[E_9]$ anions per unit cell, exist in the cp-compound class:

1. Compounds **3e**, **3f**, **3j**, and **4d** contain four cations per cluster and thus the charge of the anions is unambiguously four.
2. Compounds **2e**, **2f**, **3g**, **3h**, and **4e** contain clearly three cations per cluster and thus the cluster has a three-fold negative charge.
3. Compounds **2g**, **2h**, **2i**, **3i**, and **4f** contain six cations and two separated cluster anions and thus an average charge of -3 per cluster. In principle a disproportion in $[E_9]^{2-}$ and $[E_9]^{4-}$ clusters is possible and was suggested for **2i**. The arguments are based solely on the different shapes of the two individual clusters. Since one cluster has C_{4v} symmetry, the charge allocation was set to $4-$. However, the atoms of the open square have relatively high dislocation parameters, which indicates local disorder (see Section 5.1). Magnetic data for the related Sn and Pb compounds **3i** and **4f**, respectively, give a strong indication that the clusters are partially disproportioned and coexist with three different charges $2-$, $3-$ and $4-$ (see Section 6.2).

In all crystals, that contain clusters with an average charge of $3-$ (**2e**, **2g**, **2h**, **2i**, **3h**, **3i**, **3j, 4e** and **4f**), the K-cp units form a packing with channels for the cluster anions [30,49]. This packing is observed despite different crystal symmetry, different kind and number of solvent molecules.

3.4.2. $[K\text{-}cp]_m(Cs)_n[E_9]\ (en)_p$ (E = Ge, Sn) from ternary phases

There are two compounds which possess two kinds of alkali metals each. The compounds $[K^+\text{-}cp]_2(Cs^+)_4([Ge_9]\text{-}[Ge_9])^{6-}(en)_6$, **2j**, and $[K^+\text{-}cp](Cs^+)_7\ ([Sn_9]^{4-})_2\text{-}(en)_4$, **3j**, are obtained by dissolving ternary alloys of the composition Cs_2KE_9 (E = Ge, Sn) in en. Crystallisation with cp leads for Ge to oxidative coupling of two $[Ge_9]^{4-}$ clusters. Like the formation of **2d**, no oxidation reagent was used and the oxidation was probably caused by impurities. The details of the structure **2j** including the dimer unit $([Ge_9]\text{-}[Ge_9])^{6-}$ are shown in Fig. 2d. The dimer has a crystallographic centre of symmetry at the midpoint of the exo-bond connection. The cluster linkage of 2.49 Å is shorter than intracluster atom contacts and indicates a localised two-centre–two-electron bond. The unit has direct contact with overall four Cs atoms. One type of Cs atoms bridges two almost parallel edges of the two Ge_9 clusters of the dimeric unit. The other Cs atom type sits above the rectangular cluster face of one $[Ge_9]$ unit, and bridges a polyhedral edge of the second part of the dimer.

There is an interesting similarity between the orientation of two clusters in **2j** and **3j**. During crystallisation of **3j**, $[Sn_9]^{4-}$ anions are not oxidised and are maintained in the crystal. The structure reveals that the cp-sequestered K atoms are ordered in layers, which separate two-dimensional slabs of the composition $(Cs^+)_7([Sn_9]^{4-})_2$ (Fig. 2e). The relative orientation of the clusters and the coordination sphere around the exo-bond of the dimer is similar to the arrangement of the ions in **2j**. Two clusters in the two-dimensional slabs of **3j**, which are related by symmetry, are bridged by two kinds of Cs atoms. One kind bridges two vertices of neighbouring Sn_9 clusters, the second kind bridges a rectangular face of one cluster and a triangle of a second $[Sn_9]^{4-}$. Consequently, the two $[Sn_9]^{4-}$ clusters shown in Fig. 2e have a relative arrangement, which resembles the orientation of the two Ge_9 of the dimer in **2j**. However, the intercluster distance between the corresponding Sn atoms is 4.67 Å and thus considerably longer than intracluster distances.

Oxidative coupling of Zintl anions was recently shown also for $[P_{11}]^{3-}$. Using $[Br_2]^-$ in liquid ammonia as an oxidation reagent leads to the dimer $[(P_{11})\text{–}(P_{11})]^{4-}$, which consists of two trishomocubane-like cages connected by a single bond [50].

4. Chemical bonding and electronic structures of nine-atom polyhedra

4.1. Wade rules

The enhanced stability of polyhedra with predominant deltahedral faces is well understood for boranes and carboranes. As known from molecular orbital theory for deltahedra, the number of bonding orbitals can be divided into two orbital groups: orbitals that are mainly localised in the polyhedral framework or orbitals that are localised in external bonds. According to Wade rules a n-vertex polyhedron $(B\text{–}H)_n$ has n bonding orbitals of the external B–H bonds and $n+1$ bonding cluster-skeleton orbitals [51]. Consequently, such a polyhedron is stable with $2n+(2n+2)=4n+2$ electrons. Since the atoms B and H contribute 3 and 1

electron per vertex, respectively, and thus $4n$ electrons to an n vertex cluster, a stable *closo* deltahedron should appear with two negative charges ($4n+2$ electrons). The rules can be extended to ligand-free polyhedra if external bonds are substituted by non-bonding electron pairs (lone pairs). The substitution of the four electron unit B–H by the iso(valence)electronic one-atom unit E (E = Group 14 atom) leaves the number of valence electrons unchanged and all clusters $[(BH)_n]^{2-}$ should have a counterpart $[E_n]^{2-}$. Noticeably the cluster charge -2 is independent of cluster size n.

If one, two or three vertices of a deltahedron are removed, the number of bonding skeletal orbitals remains unchanged and the resulting clusters are *nido*, *arachno*, or *hypo*-type, respectively. Each missing vertex requires two additional electrons to fill all bonding orbitals, which means that starting from a *closo*-$[E_n]^{2-}$ we obtain *nido*-$[E_{n-1}]^{4-}$, *arachno*-$[E_{n-2}]^{6-}$, and *hypo*-$[E_{n-3}]^{8-}$ clusters. Since n is arbitrary we expect *closo*-$[E_n]^{2-}$, *nido*-$[E_n]^{4-}$, *arachno*-$[E_n]^{6-}$, and *hypo*-$[E_n]^{8-}$ clusters. An optimum certainly exists between the number of vertex n and the charge distributed over the n atoms. It can be expected that higher charges will be better realised with large n, because the charge is distributed over more atoms. The existence of the large number of stable $[E_9]^{x-}$ clusters with $x = 3$ and 4 shows, that an average, atom charge between 0.33 and 0.44 corresponds to a 'good' value. Clusters with lower charges should be stable as well. Crystalline products with single charged clusters are not known, probably because no counter-ions with the perfect size to form stable 1:1 crystals are available. In the gas phase, however, single and double charged anions can be observed (see Section 6.3).

4.2. Frontier orbitals and quantum mechanical calculations

There are two types of basic, almost spherical polyhedra, which can be constructed from nine-atoms: the tri-capped trigonal prism **I** with D_{3h} point group symmetry and the mono-capped square anti-prism **II** with C_{4v} point group symmetry (Fig. 4a). The polyhedra **I** and **II** correspond to *closo*- and *nido*-polyhedra, respectively, and are connected by Eulers theorem $n_V + n_F - n_E = 2$, where n_V is the number of vertices, n_F is the number of polyhedron faces and n_E is the number of polyhedron edges. Flattening the bent rectangle 1–3–2–4 along 1–2 in **I** leads to the loss of the edge 1–2, and the two triangles 1–2–3 and 1–2–4 merge to the square 1–3–2–4 in **II**. Thus the value of the term $n_F - n_E$ of Euler's theorem remains unchanged by this transformation.

From Wade rules *closo*-structure **I** should be favoured for clusters with 20 skeletal electrons and *nido*-structure **II** with 22 skelatal electrons or 38 and 40 valence electrons, respectively, including the lone pairs at each vertex. The structures are closely related and the conversion of nine-atom clusters takes place already at room temperature, as was proven by NMR experiments. Rudolph et al. showed [52,53] that $[Sn_9]^{4-}$ and $[Pb_9]^{4-}$ anions in solution have only one NMR signal (^{119}Sn or ^{207}Pb), i.e. that all atoms are equal on the NMR time scale and that the polyhedral skeleton is very flexible. In comparison to this, the conversion of isoelectronic boranes and carboranes affords much higher temperatures [54].

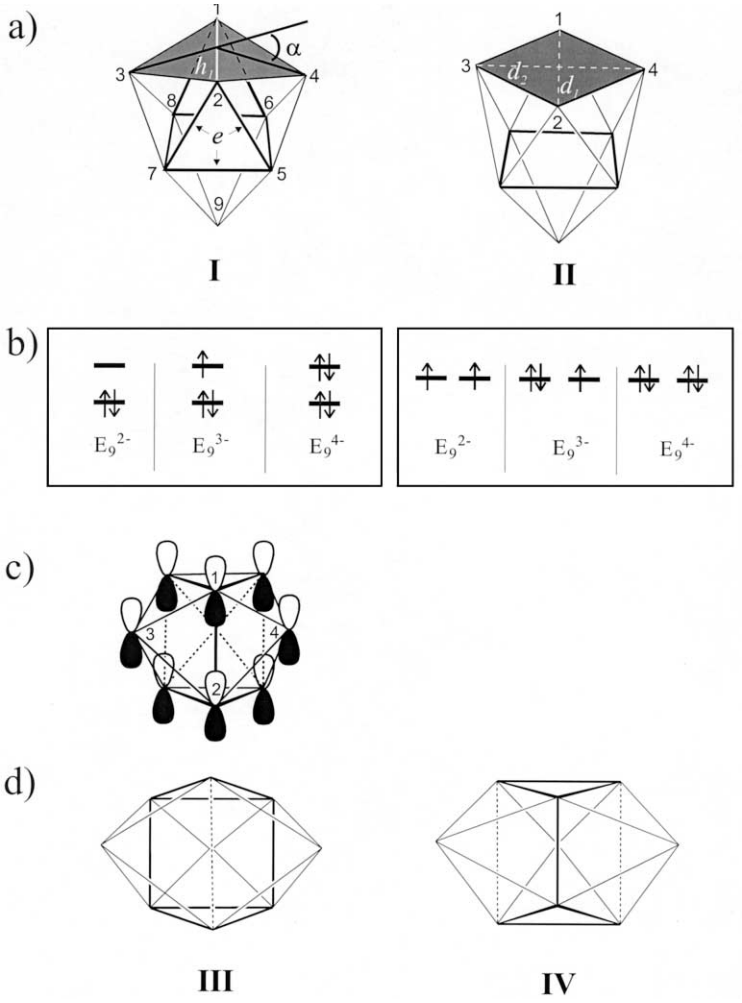

Fig. 4. (a) Parameters for the description of the ideal structures **I** and **II** and distortions from D_{3h}- and C_{4v}-symmetry, respectively, towards C_{2v} symmetric intermediates. Values are given in Table 1. (b) Electron occupation of the frontier orbitals of 20, 21 and 22 skeletal electron clusters with structure **I** (left) and structure **II** (right). (c) Molecular orbital of the LUMO of a 20 electron cluster with D_{3h} symmetry. (d) Two possible structures for intermediates with C_{2v} symmetry. Distortion of the trigonal prism in **I** can lead to **III** with one longer and two shorter prism heights and vice versa to **IV**.

A D_{3h} symmetric nine-atom cage with 20 skeletal electrons (e.g. *closo*-$[B_9H_9]^{2-}$ or $[Sn_9]^{2-}$) possess a LUMO which is bonding along the edges *e*, but anti-bonding along the heights *h* of the trigonal prism (Fig. 4b and c) [55]. Occupation of the LUMO with one or two further electrons, as it is the case for $[E_9]^{3-}$ and $[E_9]^{4-}$ anions, respectively, should lead to a distortion of the cluster **I** towards larger h/e values in comparison to an ideal polyhedron with equal edge lengths ($h/e = 1$) [56]. Continuous elongation of only one prism height and relaxation of the other atoms

transforms polyhedron **I** via a C_{2v} intermediate **III** to **II** (Fig. 5a). The HOMO of a C_{4v} symmetric nine-atom cage **II** with 22 skeletal electrons (*nido* type) is degenerate (Fig. 4b). Oxidation of the $[E_9]^{4-}$ cluster leads to an unsymmetrical occupation of the HOMO in $[E_9]^{3-}$. According to Jahn and Teller the system can lift the degeneracy and lower the energy by distortion towards a molecule with lower symmetry. In the case of small electron–electron interactions the distortion instead of a triplet state can occur for a C_{4v}-symmetric polyhedra $[E_9]^{2-}$. Shortening of one diagonal in **II** according to stretching modes leads to polyhedron **III** or **III′** with C_{2v} symmetry and finally to **I** or **I′** (Fig. 5a).

Qualitative quantum mechanical calculations on the Extended Hückel level reveal the HOMO–LUMO situation for $[E_9]^{4-}$ and $[E_9]^{2-}$ (E = Ge to Pb) shown in Fig. 4 and predict that the *nido*-C_{4v} conformation and *closo*-D_{3h} structure, respectively, are favoured as predicted from Wade rules [57]. Calculations on HF level show that the configuration with C_{4v} symmetry **II** corresponds to the minimum in energy of $[Si_9]^{4-}$. Configuration **I** is destabilised only by 2.5 kJ mol^{-1}, but represents a degenerate transition state [34]. Since in solid state none of the clusters has ideal D_{3h} point group symmetry the degeneracy should be lifted in all cases. Density functional calculations carried out for $[Pb_9]^{4-}$ and $[Pb_9]^{3-}$ show that *nido*-C_{4v} conformation **II** and C_{2v}-conformation **III**, respectively, are found at the minimum. The skeleton of $[Pb_9]^{4-}$ is quite flexible as it can be seen by the analysis of the vibrational frequencies [58].

4.3. Intramolecular rearrangements in nine-atom clusters

The smooth process shown in Fig. 5a and as described in Section 4.2 elucidates the relationship between the cluster types **I** and **II**. The conversion process allows the exchange of capping atoms and atoms of the trigonal prism. The capping atom 3 in **I** is part of the trigonal prism in isomer **I′**. Consequently, this least-motion-process also describes the rearrangement of atoms of cluster type **II**, and is generally known as *diamond-square-diamond* mechanism. Consecutive conversions allow all atoms in the two boundary structures **I** and **II** to exchange with each other.

It was pointed out early [54] that an electronic factor is operative in raising the rearrangement barrier for $[B_9H_9]^{2-}$ via the C_{4v} intermediate **II**. The electronic state for 20 and 21 skeletal electron clusters is degenerate under C_{4v} symmetry as can be deduced from the occupation of the HOMO e^2 or e^3 (Fig. 4b). Therefore it was expected that rearrangement of 20 and 21 electron D_{3h} clusters is not likely via a C_{4v} intermediate. An alternative least-motion-process shown in Fig. 5b avoids the high symmetric intermediate **II** [56]. Stretching of polyhedral edges 1–2 and 6–8 of the D_{3h} model **I** leads to polyhedron **IV** with C_{2v} symmetry via a C_s symmetric intermediate. **IV** is a trigonal prism with two elongated prism heights (3–4 and 6–8) and one short height (5–7). In comparison, **II** has one long and two short heights. Relaxation of the atoms leads to the isomer **I′**, where again capping atoms and atoms of the trigonal prism are exchanged.

The shapes of the two superposed anions **B** and **C** shown in Fig. 6 [59] demonstrate a third possibility of cluster conversion via a low symmetry path.

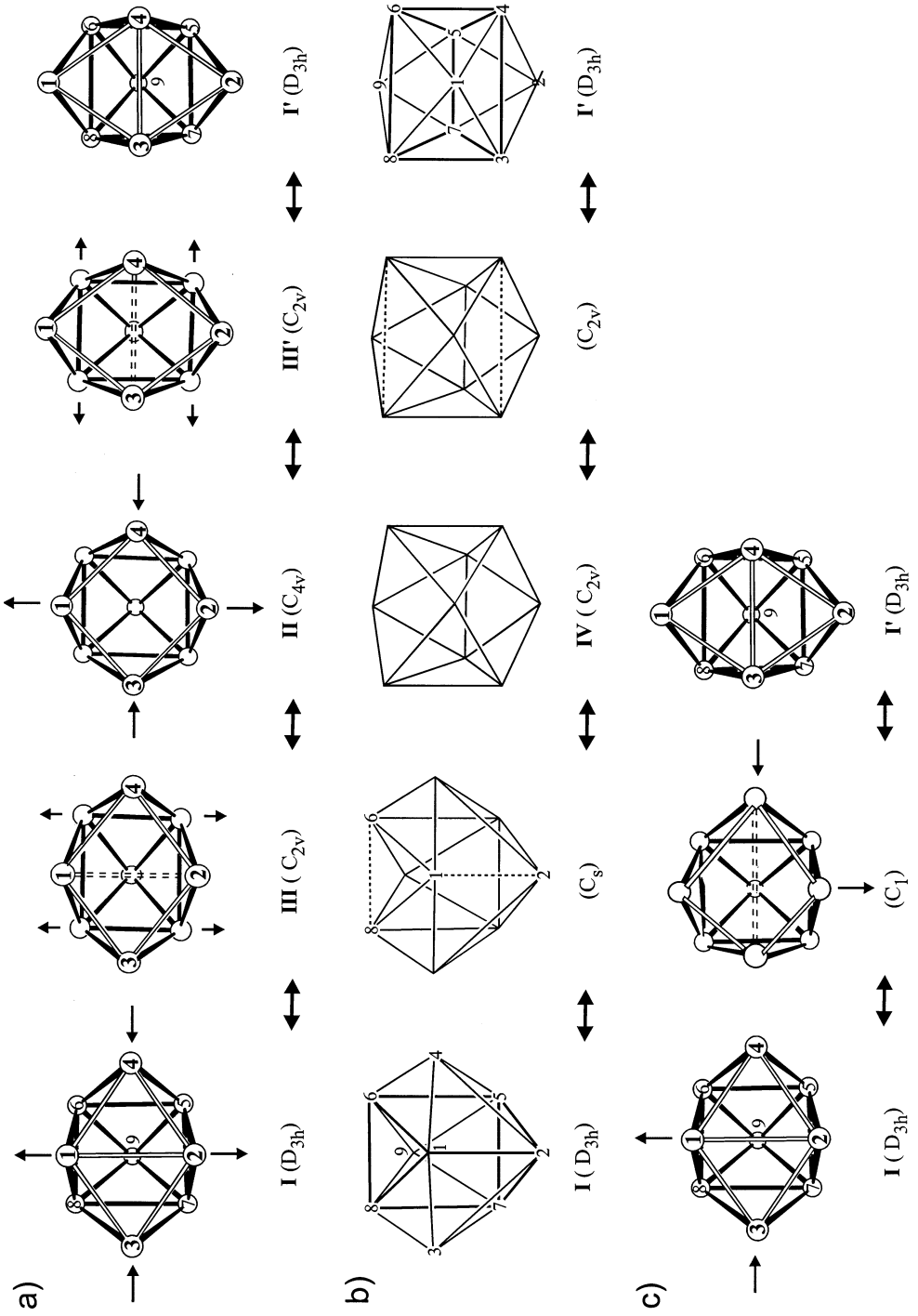
a)
b)
c)
I (D3h)
II (C4v)
III (C2v)
III' (C2v)
I' (D3h)
I (D3h)
III (C2v)
(C2v)
IV (C2v)
(Cs)
I' (D3h)
I (D3h)
(C1)
I' (D3h)

Fig. 5.

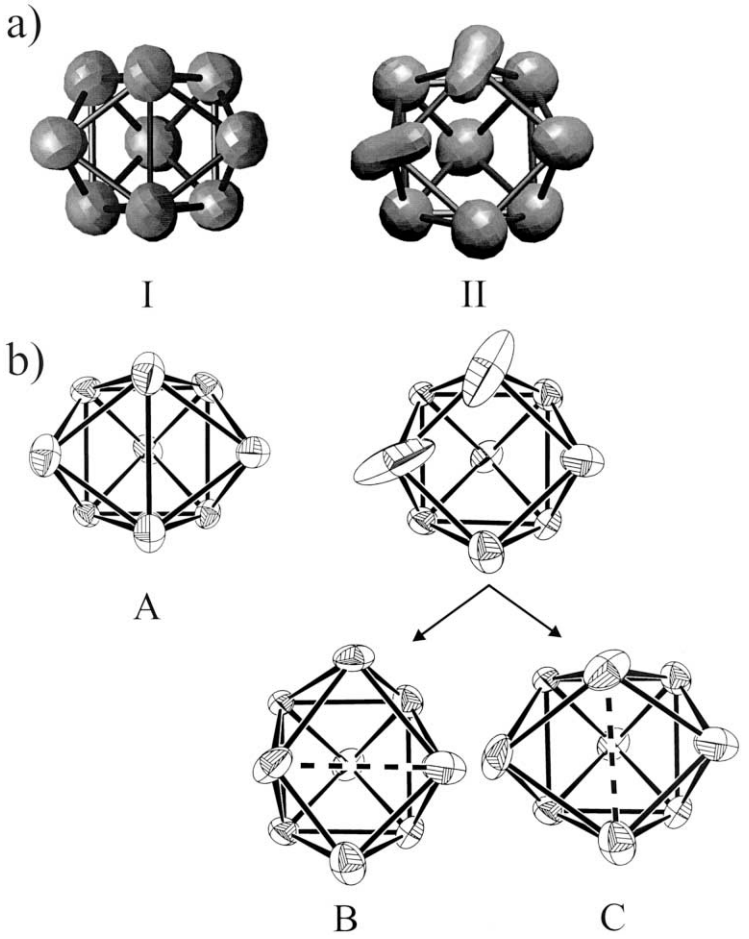

Fig. 6. View of $[Sn_9]^{3-}$ anions in **3i**. (a) Experimental equi-electron density (one-sixth of the maximum of the observed electron density) surface in the region of the cluster **A** and the two superposed clusters **B** and **C**. (b) The large ellipsoids are described with two split positions of atoms, each with atom site population of 0.5. As result two distorted tricapped trigonal prisms oriented perpendicular to each other are found. The average structure of the superposition of **B** and **C** pretend cluster **II** with almost perfect C_{4v} symmetry. All thermal ellipsoids are shown at 50% probability level [59].

Shifting the atom pair 1–3 in **I** leads to a C_1 symmetric polyhedron with the shape of **B**. Consecutive shift of the atom pair 2–4 leads to the approach of atoms 3 and 4 and thus to the isomer trigonal prism **I′** (Fig. 5c) [60].

Fig. 5. (a) Transition between the two boundary structures **I** (D_{3h}) and **II** (C_{4v}) via the *diamond-square-diamond* mechanism which allows all atoms to exchange. (b) Alternative rearrangement process by simultaneous stretching of two polyhedral edges. (c) Rearrangement of cluster atoms as indicated from structure **B** and **C** in Fig. 6.

5. Shapes of homoatomic nine-atom clusters

5.1. Structure determination from X-ray diffraction of single crystals

X-ray structure determination of single crystals is the most widely used method to resolve the shape of the anions. The structures of a large number of anions are known and the results are summarised in Table 1. EXAFS methods are not sufficient to resolve the different isomers (see Section 5.2). Fourteen crystal structure refinements out of 29 listed in Table 1 converge with rather high R-values ($R_1 > 0.08$), thus the data must be carefully analysed. X-ray structure determination of nine-atom clusters can even feign a wrong structure of the anions. As in the case of the structure determination of the anion $[B_9H_9]^{2-}$ in $Rb_2B_9H_9$ [61], the superposition of model **I** and **I′** can lead to an average structure **II**. Using the C_{4v} symmetric model **II** during structure refinement leads, however, to elongated ellipsoids of the atoms of the open square. In the case of $Rb_2B_9H_9$, the four dislocated atoms fit well with two superposed D_{3h} symmetric clusters. A similar, but different situation was found for **3i** and the isotypic compound **4f** [59]. The compounds contain two symmetry independent clusters and six counter ions. The electron density map from a Fourier analysis reveals the three-dimensional surface shown in Fig. 6a. Cluster **A** is ordered and appears as an approximate C_{2v} symmetric cluster of type **III** (Fig. 6b). The second cluster shows two noticeable large areas for two atoms of the open square of an assumed cluster type **II**. The anisotropic electron density around the two atom positions in **3i** and **4f** can be resolved is better described by superposition of two clusters of type **B** and **C** of approximate C_s or true C_1 symmetry (Fig. 6b).

5.2. Structure determination from EXAFS data

The calculation of mean atom-to-atom distances for clusters **A** and **B** in $[K\text{-cp}]_6[Ge_9Ge_9](en)_{0.5}$ (**2g**) shows that the distance range can be mainly devided into two groups, namely 2.6–2.9 Å and 4.0–4.2 Å (Fig. 7a). The values reflect nearest and next-nearest neighbour contacts. All values, which lie between the two groups correspond to long prism heights of cluster type **III**. The Fourier transformation of the EXAFS spectra of a powdered sample of once larger single crystals of **2g** show a peak between 2.0 and 3.0 Å and further peaks between 3.0 and 5.0 Å (Fig. 7b) [62]. Peak fitting for smaller distances requires two Ge–Ge shells, the peaks at larger distances need three shells in order to give a satisfying fit. Fig. 7c shows the distance histogram as calculated from EXAFS data. The distances correlate quite well with the histogram obtained from atom parameters of the single crystal structure determination shown in Fig. 7a. The five shells from EXAFS data reveal two groups of distances around the mean values of the X-ray data and two values with lower frequency at distances between the two groups. The results show that EXAFS can serve as a significant tool for the analysis of the clusters in solid state, and open the possibility of the investigation of non-crystalline materials. However, EXAFS cannot resolve small distortions of the polyhedra.

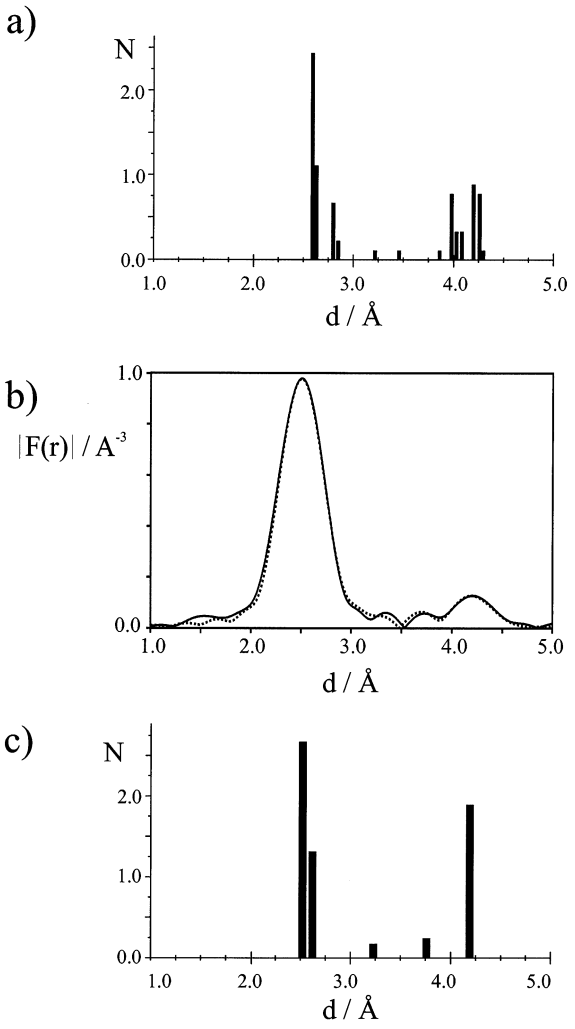

Fig. 7. (a) Distance histogram of Ge-Ge contacts obtained from X-ray diffraction of single crystals of $[K\text{-}cp]_6[Ge_9Ge_9](en)_{0.5}$ (**2g**). (b) Fourier transformed EXAFS spectrum of **2g**: experimentell (solid) and theoretical (dotted) k^3-weighted EXAFS-function. (c) Distance histogram obtained from EXAFS analyses [62].

Belin et al. calculated mean atom-to-atom distances for cluster **A** and **B** in **2i** and found that apart from the distance of 3.61 Å (cp. d_1 in Fig. 4a) the values do not significantly vary. Introduction of this contribution during the EXAFS analysis of data, which are obtained from an en solution of an alloy of the stoichiometry $KGe_{1.8}$, gave a slight preference for the C_{4v} model of cluster **B**, but it was not possible to exclude equilibrium between the two species in solution [63].

5.3. Cluster types

All nine-atom clusters appear with almost spherical or elliptical shape. In order to define distances between nearest neighbours and to compare the shapes of the anions which consist of different atom types, torsion angles, length ratios and scaled bond lengths are chosen for the discussion. The clusters are discussed in terms of the two boundary structures **I** and **II** with D_{3h} and C_{4v} symmetry, respectively (Fig. 4). Both types can be described using the parameters h_i ($i = 1–3$), e, γ and α_i ($i = 1–3$) as shown in Fig. 4a: The central unit in **I** is a trigonal prism which is characterised by three prism heights $h_1 = d(1–2)$, $h_2 = d(5–6)$, or $h_3 = d(7–8)$, basal edges e and the angle between opposed triangular prism faces (angle between the two planes 1–6–8 and 2–5–7). Elongation or compression of the prism is expressed by larger and smaller h/e ratios, respectively. The topology of the capping atoms 3, 4, and 9 in **I** can be described by cap-to-cap fold angles about each prism edge h (e.g. 1–2–3/1–2–4) or the dihedral angles α_1 to α_3 (180° minus cap-to-cap fold angle). A distortion from three-fold symmetry in **I** is expressed by different prism heights. There are two conformations with C_{2v} symmetry: **III** has one short and two long heights, **IV** has one long and two short heights (Fig. 4d). Three different heights enforce C_s symmetry (cluster type **V**). As a result of different prism heights, opposed triangular prism faces deviate from coplanarity ($\gamma \neq 0$). Different prism heights correlate also with different dihedral angles α_1 to α_3. Clusters with D_{3h} point group symmetry (type **I**) must have equal fold angles. The least motion process in Fig. 5a makes clear that one elongated height correlates with small α. Configuration **II** is the boundary structure with one elongated height (h_1) and α_1 equal to 0; h_1 becomes one of the diagonals (d_1) of the open square. For **II** with ideal C_{4v} point group symmetry α_2 and α_3 are equal. If the cluster is regarded as a monocapped quadratic antiprism **II**, α also characterises the deviation from planarity of the open square 1–2–3–4. Starting with the description from boundary structure **II**, deviations from C_{4v} symmetry show up in different diagonal lengths $d_1 = d(3–4)$ and $d_2 = d(1–2)$ of the open square 1–3–2–4 (Fig. 4). In order to classify the distortions of **II** towards **I** the shorter diagonal is chosen as third prism edge.

The clusters are allocated to the following types by inspecting Table 1 on the basis of the above mentioned parameters:

type **I** with D_{3h} symmetry (tricapped trigonal prism),
type **II** with C_{4v} symmetry (monocapped square antiprism),
type **III** with C_{2v} symmetry (tricapped trigonal prism with one elongated prism height),
type **IV** with C_{2v} symmetry (tricapped trigonal prism with two elongated prism heights) and
type **V** with C_s symmetry (tricapped trigonal prism with three different prism heights). Type **V** may also have C_1 symmetry.

There exists only one polyhedron of type **I** with almost perfect D_{3h} symmetry. The 21 skeletal electron cluster $[Sn_9]^{3-}$ in **3g** has approximately three equal prism heights which differ by less than 2%, three equal cap-to-cap fold angles and $\gamma = 1°$.

Polyhedra of approximately type **II**, i.e. with a difference in diagonal lengths of less than 5%, are realised for Ge in **2a** (**A**, **B**), **2b**, **2c** (**A**), and **2i** (**B**); for Sn in **3e**, **3f**, **3j**, and 3**k**; as well as for Pb in **4a** (**A**), **4b**, **4c**, **4d**, and **4g**. Polyhedron **B** in **4a** has $d_1/d_2 = 1.05$, but $\alpha_1 = 17°$ instead of 0° expected for C_{4v} symmetry. Therefore, this cluster is allocated to type **IV**. Polyhedron **D** in **2a** has $d_1/d_2 = 1.07$ and $\alpha_1 = 6°$, thus this structure is still close to C_{4v} symmetry. In case of perfect C_{4v} symmetry α_2 and α_3 are equal. With the exception of **2a** (**B**) and **2i** (**B**) is $\alpha_2 = \alpha_3 \pm 5°$. α_2 and α_3 differ by 10° and 8° for **2a** (**B**) and **2i** (**B**), respectively. All polyhedra of type **II** possess 22 skeletal electrons with the exception of **2i**, where the electron number cannot be determined unambiguously, because there are two independent Ge_9 clusters per unit cell. There are no Si clusters with undistorted C_{4v} symmetry. Cluster **A** in **1a** differs significantly from C_{4v} symmetry as can be seen from $d_1/d_2 = 1.08$ and $\alpha_1 = 9°$. Interestingly, polyhedra of type **II** are mainly observed for clusters of the heaviest element Pb.

Polyhedra where one prism height is elongated by more than 5% if compared to the two other prism heights, which differ by less than 5%, are assigned to cluster type **III**. In case of C_{2v} symmetry, two cap-to-cap fold angles must be approximately equal ($\alpha_2 = \alpha_3 \pm 5°$). This type is most frequent and occurs in **2a** (**C**), **2c** (**B**, **C**), **2d**, **2g** (**A**, **B**), **2h** (**A**), **2i** (**A**), **2j**, **3d**, **3h**, **3i** (**A**), **4e**, and **4f** (**A**). Clusters **B** and **C** in **3i** and **4f** are of type **III** with respect to prism heights, but have lower symmetry than C_{2v}, due to large differences in cap-to-cap fold angles, and are therefore assigned to type **V** with C_1 symmetry.

There are five examples of cluster type **IV**. In **1a** (**B**, **D**), **2f**, **3b**, and **4a** (**B**) two prism heights differ by less than 5% and are elongated by at least 10% if compared to the 3rd prism height. There are also two cap-to-cap fold angles with approximately the same values ($\alpha_1 = \alpha_2 \pm 3°$), which are considerably smaller than the third one. **2f** is a 21-electron, the others are 22-electron clusters.

Three different prism heights are present in **1a** (**A**, **C**), **2e**, **3a**, and **3c**. The heights in **3c** are most balanced and differ by less than 4%. Cluster **A** in **1a** has the most imbalanced heights; h_2 differs from h_1 by 18% and from h_3 by 8%, respectively, and is assigned to type **II**.

5.4. Correlation between cluster shapes and electron numbers

The interatomic distances along the edges of anionic nine-atom polyhedra are elongated for Si and Ge with respect to the distances in the element structures (α-Si 2.35 Å, α-Ge 2.45 Å) or in molecules with two-centre–two-electron bonds (see legend of Fig. 1). For Sn the atom-to-atom contacts of the anions are elongated with respect to α-Sn (2.81 Å) and are in the range of those in β-Sn (3.01–3.18 Å). For Pb the distances are shorter than in fcc-Pb (3.50 Å) due to the higher coordination number 12 of the atoms in the element structure. The bond length distribution of the anions is much larger than of the cage compounds in Fig. 1a.

From Wade's rules one predicts that 20-electron clusters adapt structure type **I**. Addition of electrons leads to elongation of prism heights and finally to **II**. There are only few examples of polyhedral anions that have a structure close to **I**. The

undistorted $[B_9H_9]^{2-}$ has three equal heights and consequently the triangular edges of the prisms are co-planar (Table 1). The three equal bond angles α represent almost the ideal three-fold symmetry of the capping atoms 3, 4, and 9. The value of the h/e ratio (0.96) agrees with the MO picture, i.e. the LUMO, which is antibonding along the prism heights in this case, is not occupied (Fig. 4c). There have been several reports on 20-electron clusters $[E_9]^{2-}$. It is assumed that $[Ge_9]^{2-}$ exists [63], but no structure refinement has been reported so far. There are indications that $[Ge_9]^{2-}$ appears in brown crystals [43,60] which have the same cell parameters and space group as the violet $[K\text{-cp}]_2Ge_{10}$ [14]. Crystals of the brown compound contain two ordered K-cp units, but the structure and composition of the anion was not resolved due to disorder. Because of the high molecular mass, data from elemental analysis are not reliable to distinguish between the presence of $[Ge_9]^{2-}$ and $[Ge_{10}]^{2-}$. Certainly the structure of the brown crystals differs from the violet ones, since it was not possible to verify the disorder model of two superposed $[Ge_{10}]^{2-}$ conformers [43,60].

Interestingly, the paramagnetic $[Sn_9]^{3-}$ in **3g** and the 22-electron cluster $[Bi_9]^{5+}$ in $Bi_{10}(HfCl_6)$ have almost perfect D_{3h} symmetry (type **I**) [64] and as expected for clusters with more than 20 electrons both anions have elongated prism heights with $h/e = 1.08$ and 1.15, respectively. $[Sn_9]^{3-}$ and $[Bi_9]^{5+}$ clusters occur also in other compounds with different shapes. **3h** differs from **3g** just by one en molecule per formula unit, but the $[Sn_9]^{3-}$ cluster in **3h** is significantly distorted. It has the same h/e ratio as in **3g**, but adapts type **III** with one height elongated by 10%. In $Bi_{12}Cl_{14}$ (Table 1) [65], $[Bi_9]^{5+}$ also adapts structure **III** with $h/e = 1.19$. One prism height is elongated by 7%. But D_{3h} structure **I** is observed for 18-electron clusters $[B_9X_9]$ ($X = Cl$, Br; $2n$ skeletal electrons). Here the occupation of fewer orbitals, which are bonding along the prism heights, leads to larger h/e ratios [66,67].

Twenty-two-electron cluster anions $[E_9]^{4-}$ should have the *nido*-structure **II**. However, only few examples adapt to the C_{4v}-symmetric configuration. Inspecting the d_1/d_2 ratio, $R_{b12}Si_{17}$ only one (**A**) of four clusters is close to C_{4v} symmetry ($d_1/d_2 = 1.08$). The others (**B**, **C**, **D**) are better described as species derived from **I** with two long and one short or three different prism edges. Independent of the distortion is $h/e > 1.15$. Comparable h/e values are observed for all non-C_{4v} symmetric 22-electron clusters $[Ge_9]^{4-}$ with the exception of the linked clusters of the polymer chain in **2d** which has rather small h/e. In $-([Ge_9]^{2-})_n-$ the clusters have 22 skeletal electrons, seven lone pairs and one electron for each of the two exo-bond. The h/e value of 1.07 in **2d** is smaller than the ones observed for $[Ge_9]^{3-}$ anions, even the orbital in Fig. 4c is occupied with two electrons in case of **2d** and with one electron for $[Ge_9]^{3-}$ anions. The distortions of the anions in **2d** (22 el.), **2j** (22 el.) and **2e** to **2i** (21 el.) are very similar and correspond to a compression of structure type **II** along 1–2 (Fig. 4a), but without relaxation of the atoms 3 and 4 and thus keeping α_1 close to 0°. Just in cases in which $[Ge_9]^{3-}$ anions occur as discrete units and where no second independent cluster is present in the unit cell, the three cap-to-cap-fold angles reflect a distortion towards D_{3h} symmetry. Several examples of 22-electron clusters of type **II** exist for Sn and Pb. Exceptions are again of type **III** (**3d**), type **IV** (**3b**), and **V** (**3c**). Especially, $[Sn_9]^{4-}$ in **3c** shows a similar distortion than $[Sn_9]^{3-}$ anions.

In summary, there is no obvious rule which helps to determine the shape of the anions. The outstanding parameter is the h/e value i.e. 22-electron clusters generally have larger h/e than 21-electron clusters.

6. Properties of homoatomic nine-atom clusters

6.1. Raman spectroscopy

$[E_9]$, $[E_5]$, and $[E_4]$ clusters show typical lines in the Raman spectrum [32,34,48,68,69]. For a nine-atom species with C_{4v} symmetry one expects 21 fundamentals with 20 Raman active modes. Generally four to five broad bands are observed, a phenomenon that was attributed to accidental coincidences and low intensities. Therefore Raman spectroscopy of solid samples cannot be used for an analysis of small cluster distortions as they are observed using X-ray diffraction methods, but they can prove the presence of the various clusters in single crystals, powders, in non-crystalline samples and in solution.

The thermal decomposition of CsSi was studied by Raman spectroscopy. First it leads to a compound containing $[Si_4]$ and $[Si_9]$. At higher temperatures only $[Si_9]$ is present (Cs_4Si_9) which can be observed by the increasing intensities of the characteristic lines at 250 cm^{-1} (very weak), 295 cm^{-1} (weak), and 386 cm^{-1} (strong). $[Si_5]$ clusters are not observed during the reaction [34]. The presence of both four- and nine-atom clusters is also observed in the binary phases $A_{12}E_{17}$ (A = K, Rb, Cs; E = Ge, Sn). Nine-atom clusters are exclusively present in A_4Ge_9 (A = K, Rb, Cs) and A_4Sn_9 (A = K, Cs). The characteristic, strongest line shifts from 386 cm^{-1} for Si_9, to 220 cm^{-1} for Ge_9 and to 152 cm^{-1} for Sn_9. The Raman spectra show the same trend as the tetrahedral anions with 475 cm^{-1} for Si_4, 274 cm^{-1} for Ge_4, and 185 cm^{-1} for Sn_4 [32].

6.2. Magnetic properties

As pointed out above, the structure–property relationship of nine-atom clusters is of specific interest. The anions occur with different charges and the paramagnetic $[E_9]^{3-}$ species are rare examples of main-group element radicals. Several compounds which contain $[E_9]^{4-}$ anions are diamagnetic. The diamagnetism was revealed using a SQUID magnetometer for $Rb_{12}Si_{17}$, Cs_4Ge_9, and Cs_4Pb_9 and a Faraday balance for $Na_4Sn_9(en)_7$. Positive, but temperature independent magnetic susceptibility is reported for $[K\text{-}cp]_2(Cs)_4([Ge_9]\text{–}[Ge_9])(en)_6$, **2j**. No EPR signal was observed for a powdered sample of K_4Pb_9.

More interesting are the results if unpaired electrons are present. Several compounds which contain $[E_9]^{3-}$ were investigated by EPR and SQUID magnetometer measurements. The EPR signals of powder samples and of single crystals of compounds containing $[E_9]^{3-}$ were analysed in detail for E = Ge, Sn and Pb [43]. The spectra of powdered samples of the composition $[K\text{-}cp]_3[E_9]$ (irrespective solvate molecules in the crystals) recorded at 77 K are shown in Fig. 8a. The

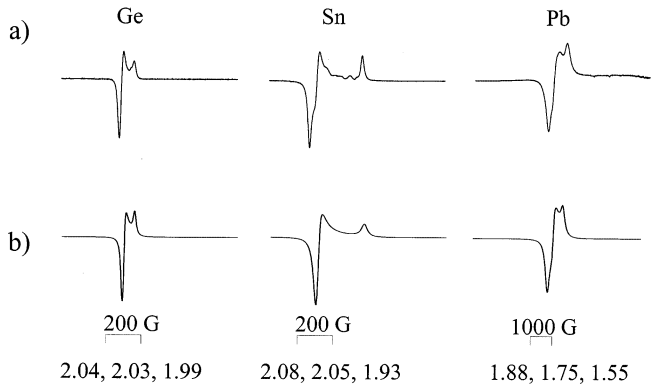

Fig. 8. (a) EPR spectra of powder samples of the composition $[K\text{-}cp]_6[E_9]$ with E = Ge, Sn, and Pb at 77 K. (b) Spectra simulation with three different g-tensor components. The g-values and line width are given at the bottom of the figure [43].

simulations of the anisotropic signals using three g tensor components lead to at least two different tensor components (Fig. 8b) and indicate low symmetric $[E_9]^{3-}$ clusters. The widths of the signal increase and the g values decrease from Ge to Pb. The g values of the powders are confirmed by EPR measurements of single crystals of **2e**, **2g**, **3i**, and **4e** [43,49]. On the one hand the EPR signals of the single crystals of **2g** and **3i** verify that the compounds contain paramagnetic $[E_9]^{3-}$ clusters, on the other hand it was assumed that due to the different shapes of the two clusters in **2i**, the anions disproportionate in $[Ge_9]^{2-}$ and $[Ge_9]^{4-}$ clusters. The observation that a single crystal of **2g**, is EPR active, leads to the assumption that paramagnetic clusters are also present in compounds **2g**, **2h**, and **2i**, which differ from **2g** only by solvate molecules.

The question if the paramagnetic or diamagnetic descriptions are valid for compounds containing two independent clusters could be answered in the case of the related Sn and Pb compounds **3i** and **4f**, respectively. Magnetic susceptibility data of **3i** and **4f** were analysed using the expression $\chi_{mol} = C/(T-\theta) + \chi_0$. The compounds show Curie–Weiss behaviour with $\theta = -0.5$ K and -2.5 K for **3i** and **4f**, respectively. The small θ values show that there are almost no intermolecular interactions. The remarkable small C values and thus small magnetic moments $\mu = 1.25$ and 1.07 μ_B for Sn and Pb, respectively, are below the value expected for a spin system with $S = 1/2$. Including the EPR data for Sn and Pb (1.73 μ_B and 1.45 μ_B, respectively) leads to about 50% paramagnetic $[E_9]^{3-}$ species ($S = 1/2$) [43]. The results can be understood by inspection of the crystal structures (Fig. 6). Each, **3i** and **4f**, contain one ordered cluster **A** and a second cluster which is best described as superposition of two clusters **B** and **C** as shown in Fig. 6. The shape of **A** matches the paramagnetic cluster anion of **3h** and thus **A** was assigned to $[E_9]^{3-}$. Since many $[E_9]^{4-}$ anions have structures with lower symmetry than C_{4v} (**3a**, **3b**, **B** in **4a**), it can be assumed that clusters **B** and **C** are 4− and 2− species or vice versa. From crystallographic data it cannot be decided whether the two structures **B** and

C are superposed or whether a dynamic disorder is present. For both cases, however, it can be assumed that two clusters $[E_9]^{2-}$ and $[E_9]^{4-}$ are at the same place or that a change in valency is the origin of the disorder. The 1:1 presence of $[E_9]^{3-}$ and the pair $[E_9]^{2-}/[E_9]^{4-}$ are consistent with 50% portion of paramagnetic species.

The fact, that in mixed valent compounds electron transfer can occur between the clusters, makes them highly interesting candidates for building blocks in materials. The significance can be seen at the examples of superconducting fulleride salts A_3C_{60} (see Section 7).

6.3. Mass spectrometric investigations

Gas phase reaction and gas aggregation techniques used for the binary systems Cs/Sn and Cs/Pb show intensity maxima for the *cationic* molecules $[Cs_3Sn_5]^+$, $[Cs_3Sn_9]^+$, $[Cs_5Sn_9]^+$, and $[Cs_3Pb_5]^+$. $[Sn_{10}]^+$ is observed at low intensity. Larger clusters were not observed due to the limitation of the mass spectrometer [70–72]. Analogies to structurally characterised Zintl ions $[E_n]^{x-}$ $x = 2$–4 are obvious.

Recent time-of-flight mass spectrometric investigations show that gas phase *anions* can be easily achieved by laser desorption [73]. The ion formation strongly depends on the nature of the starting materials used for the desorption experiments and can lead to rather large *anionic* clusters of the elements Ge, Sn, and Pb without using special gas phase clustering conditions or additional ionisation processes. In order to evaluate the dependency of the gas-phase-cluster ion formation on the ability of electron transfer and thus ion formation in the precursors, the following series of samples were investigated: pure elements (E = Ge, Pb), mixtures of the elements K/Ge and K/Pb, binary phases K_4E_9 (E = Ge, Sn, Pb), en solutions of A_4E_9 (E = Ge, A = Na, K, Rb; E = Sn, Pb, A = K), and $[K\text{-cp}]_3E_9$ salts (E = Ge, Sn, Pb).

Under conditions where cluster anions from pure elements E were observed with a maximum size of six atoms and an exponential decrease of their relative intensities with increasing cluster size, much larger clusters and preferential formation of clusters of specific sizes were observed if alkali metals (K, Rb, and Cs) were present. The results of the desorption of a mixture K/Ge, the binary phase K_4Ge_9, $K_4Ge_9(en)_x$ and crystalline compounds $[K\text{-cp}]_3Ge_9$ are shown in Fig. 9a–d, respectively.

Large anionic clusters with up to 10 atoms are formed when the mixture K/Ge (Fig. 9a) and the solvate $K_4Ge_9(en)_x$ (Fig. 9c) are used as precursors. Larger clusters and clusters consisting of two kind of atoms $[KGe_{13}]^-$ and $[KGe_{11}]^-$ are observed for K_4Ge_9 (Fig. 9b) and $[K\text{-cp}]_3Ge_9$ (Fig. 9c), respectively. Interestingly, the predominant formation of mixed element clusters $[KGe_n]^-$ from K_4Ge_9 for $n = 5$, 9, and 10 correlates with stable polyhedral anions $[Ge_n]^{2-}$. This supports the idea that indeed polyhedral Zintl ions are present in the gas phase and that the formation and the stability of ions in the gas phase are closely related to the formation of clusters in binary alloys.

For E = Sn and Pb the results are similar. Maximum cluster sizes are $[Sn_{15}]^-$ from $[K\text{-cp}]_3Sn_9$ and $[Pb_{13}]^-$ from $[K\text{-cp}]_3Pb_9$. Under similar conditions cationic clusters are observed at much lower intensities and the maximum cluster size is six [73].

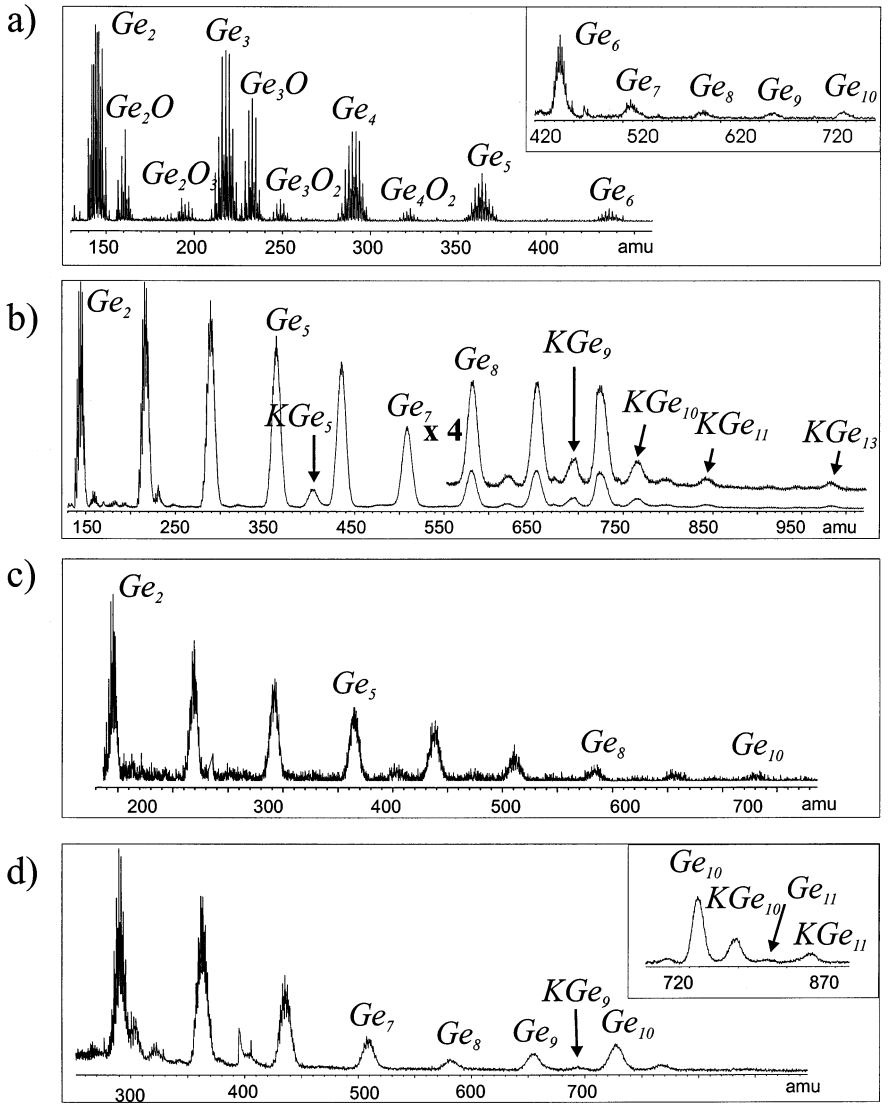

Fig. 9. Mass spectra of anions with typical isotope distributions obtained using laser desorption techniques: (a) a mixture of K and Ge; (b) K_4Ge_9, intensities of the higher mass region is four times magnified; (c) en extract of K_4Ge_9; and (d) $[K\text{-cp})]_3[Ge_9]$, the insert shows the spectrum optimised for the higher mass regions (delayed extractions) [73].

6.4. Reactivity of homoatomic nine-atom clusters

There are only few reports treating reactions with nine-atom Zintl anions. The reaction of $[E_9]^{4-}$ E = Sn and Pb with $Cr(CO)_5(THF)$ leads to the addition of $Cr(CO)_3$ to the open square of the C_{4v} symmetric cluster **II** (Fig. 3c) [74,75]. Applying the isolobal analogy, the products can be regarded as ten-atom *closo* clusters, in which the 'zero-skeletal electron' fragment $Cr(CO)_3$ occupies one vertex.

The Zintl anion $[Sn_9]^{4-}$ reacts with $[Cp(CO)_2Fe]SnBr$ to $[Cp(CO)_2Fe]_3Sn–OH$ (Fig. 3d) and the reaction with elemental tellurium leads to the insertion of Te atoms into Sn–Sn bonds under the formation of $[Te_2Sn(\mu_2\text{-}Te)_2SnTe_2]^{4-}$ (Fig. 3e). In the presence of Me_3NO the latter reaction leads to $[Sn(\mu_2\text{-}Te)_3Sn]^{2-}$ (Fig. 3f) [76].

The reaction of $[Ge_9]^{4-}$ and $Ni(CO)_2(PPh_3)_2$ in en results in $[Ge_9(\mu_{10}\text{-}Ge)Ni(PPh_3)]^{2-}$. The anion is described as a ten-atom cluster $[Ge_9Ni]$, which is centred by one Ge atom [77]. The coordination of the central Ge atom by eight other Ge atoms and one Ni atom and the distances between surface Ge atoms and the inner Ge atom is very unusual. The distance of 2.36 Å is in the range of Ge–Ge single bonds and thus very short for a Ge atom with coordination number 9.

Oxidative coupling of $[Ge_9]^{4-}$ leads to the dimer $([Ge_9]–[Ge_9])^{6-}$ and to the polymer $_\infty{}^1[Ge_9]^{2-}$ (see Section 3).

7. Comparison with alkali metal fullerides

There are several interesting similarities between homoatomic nine-atom clusters and the C_{60} 'clusters' of the lightest Group 14 element carbon:

1. $[C_{60}]$ anions occur in binary and ternary phases of alkali metals. In contrast to phases containing nine-atom polyhedra of the heavier elements, the fulleride phases with a stoichiometry close to A_3C_{60} or $A_{3-x}A'_xC_{60}$ are superconductors [9,10]. As mentioned above the critical temperature correlates with intercluster distances of fulleride anions, which are controlled by the size of the alkali ions [9,78].
2. The salts are soluble in polar solvents, the resulting anions $[C_n]^{x-}$ occur with different charges ($x = 1–6$) and disproportionation reactions of fullerides are frequent [10].
3. The LUMO of undistorted $[C_{60}]$ is degenerate and occupation of the LUMO with electrons leads to various electronic states. These states can be very close in energy and distortions are expected [79].
4. As in the case of Sn and Pb, the crystallisation of the anions of $[C_{60}]$ either with sequestering cp molecules, or with the alkali-metal complexation reagent 18-crown-6 leads to crystalline products with ordered anions. In $[K\text{-}cp]_3[C_{60}](toluene)_4$ the anions are ordered in layers with relatively large distances between the anions (Fig. 10a) [80]. In $[K\text{-}(18\text{-crown-}6)]_3[\eta^6,\eta^6\text{-}C_{60}]$ $(\eta^3\text{-toluene})_2$ all K atoms are coordinated to six O atoms of 18-crown-6 molecules. Two K atoms have contact with two hexagons of opposite faces of the fullerene

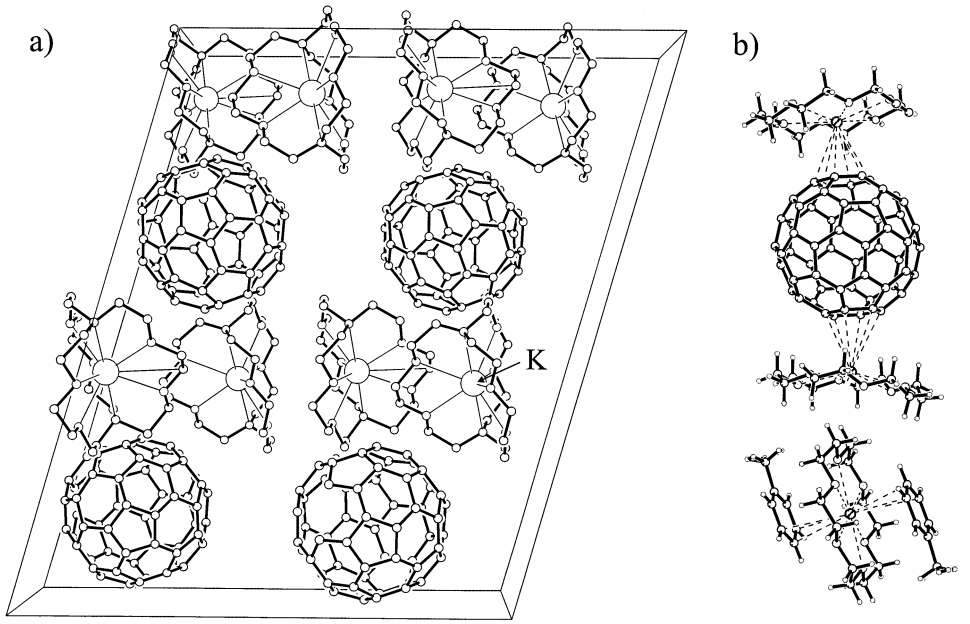

Fig. 10. Comparison of [K-cp] and [K-(18-crown-6)] salts of C_{60} and E_g anions (see also Fig. 3). (a) Crystal packing in $[K\text{-cp}]_3[C_{60}](\text{toluene})_4$ [80]. The toluene molecules and H atoms are omitted. (b) Relative orientation of $[C_{60}]^{3-}$ and $[K\text{-(18-crown-6)}]^{+}$ units in $[K\text{-(18-crown-6)}]_3[\eta^6,\eta^6\text{-}C_{60}]$ $(\eta^3\text{-toluene})_2$ [81].

molecule (Fig. 10b), the coordination shell of the third K atom is completed by two toluene molecules [81]. As for $[E_9]^{x-}$, $[C_{60}]^{x-}$ anions show an interesting and complex magnetic behaviour.

5. Polymeric fullerene chains are discussed for RbC_{60} and KC_{60} phases [82] and show a similarity to $[K\text{-cp}]_2(Cs^+)_4[Ge_9]_2(en)_6$ (**2j**) and $[K\text{-(18-crown-6)}]_2[Ge_9]$ (**2d**), where oxidation of $[Ge_9]^{4-}$ leads to the formation of the dimer $([Ge_9]\text{–}[Ge_9])^{6-}$ or the linear polymer $_\infty{}^1[Ge_9]^{2-}$, respectively.

8. Summary

Compounds with homoatomic nine-atom clusters are fascinating, because the Zintl anions $[E_9]^{x-}$ ($x = 2,3$ and 4) represent small charged particles of the respective elements E. The various distortions of the polyhedra in solid state reveal that the anions possess fluctuating skeletons. Nevertheless, the h/e ratios of the anions are related to the number of skeletal electrons. Twenty-two-electron clusters form C_{4v}-symmetric polyhedra or distorted polyhedra with enlarged h/e ratios. However, there is a large variety of possible distortions, which in some cases is similar to distortions of 21-electron clusters. Twenty-two-electron clusters of Si and Ge have an enhanced tendency to distort. The existence of mixed valent compounds

and the close relationship to the fulleride salts raise ideas that unusual electronic properties and interesting structure–property relationships can be expected for this compound class. Up to now two cases of cluster linkage by oxidative coupling are known and directed polymerisation will open tremendous possibilities for the formation of molecular semiconducting or conducting wires which are constructed from small particles of the elements.

Acknowledgements

The author wishes to thank the group of coworkers for their contributions to some of the work and for checking the manuscript. He is further indebted to C. Röhr and A.M. Guloy for making some data available.

References

[1] L. Brus, Adv. Mater. 5 (1993) 286.
[2] T. Takagahara, K. Takeda, Phys. Rev. B 46 (1992) 15 578.
[3] Y. Maeda, N. Tsukamoto, Y. Yazawa, Y. Kanemitsu, Y. Masumoto, Appl. Phys. Lett. 59 (1991) 3168.
[4] G. Schmid (Ed.), Clusters and Colloids, VCH Verlagsgesellschaft, Weinheim, 1994.
[5] M.T. Reetz, S.A. Quaiser, Angew. Chem. Int. Ed. Engl. 34 (1995) 2240.
[6] K.-L. Tsai, J.L. Dye, Chem. Mater. 5 (1993) 540.
[7] K.E. Gonsalves, H. Li, R. Perez, S.P.M. Jose-Yacaman, Coord. Chem. Rev. 206 (2000) 607.
[8] B.F.G. Johnson, Coord. Chem. Rev. 190–192 (2000) 1269.
[9] A.F. Hebard, M.J. Rosseinsky, R.C. Haddon, D.W. Murphy, S.H. Glarum, T.T.M. Palstra, A.P. Ramirez, A.R. Kortan, Nature 350 (1991) 600.
[10] M.S. Dresselhaus, G. Dresselhaus, P.C. Eklund, Science of Fullerenes and Carbon Nanotube, Academic Press, New York, 1996.
[11] M. Driess, H. Grützmacher, Angew. Chem. Int. Ed. Engl. 35 (1996) 1064.
[12] K.W.K.W. Klinkhammer, T.F. Fässler, H. Grützmacher, Angew. Chem. Int. Ed. Engl. 36 (1997) 4001.
[13] M. Stürmann, W.G. Saak, H. Marsmann, M. Weidenbruch, Angew. Chem. Int. Ed. Engl. 38 (1999) 187.
[14] C. Belin, H. Mercier, V. Angilella, New J. Chem. 15 (1991) 931.
[15] R.C. Burns, J.D. Corbett, J. Am. Chem. Soc. 104 (1982) 2804.
[16] A. Joannis, C.R. Hebd. Seances Acad. Sci. 113 (1891) 795.
[17] C.A. Kraus, J. Am. Chem. Soc. 29 (1907) 1557.
[18] C.A. Kraus, J. Am. Chem. Soc. 44 (1922) 1216.
[19] C.A. Kraus, Trans. Am. Electrochem. Soc. 45 (1924) 175.
[20] F.H. Smyth, J. Am. Chem. Soc. 39 (1917) 1299.
[21] E. Zintl, J. Goubenau, W. Dullenkopf, Z. Phys. Chem. A 154 (1931) 1.
[22] E. Zintl, A. Harder, Z. Phys. Chem. A 154 (1931) 47.
[23] E. Zintl, H. Kaiser, Z. Anorg. Allg. Chem. 211 (1933) 113.
[24] L. Diehl, K. Khodadadeh, D. Kummer, J. Strähle, Chem. Ber. 109 (1976) 3404.
[25] C.H.E. Belin, J.D. Corbett, A. Cisar, J. Am. Chem. Soc. 99 (1977) 7163.
[26] W.L. Wilson, R.W. Rudolph, L.L. Lohr, F. Parker, R.C. Taylor, D.C. Pyykkö, Inorg. Chem. 25 (1986) 1535.
[27] J.D. Corbett, Chem. Rev. 85 (1985) 383.
[28] J.D. Corbett, Struct. Bonding 87 (1997) 157.

[29] C. Belin, M. Tillard-Charbonnel, Coord. Chem. Rev. 178–180 (1998) 529.
[30] T.F. Fässler, in: P. Braunstein, L.A. Oro, P.R. Raithby (Eds.), Metal Clusters in Chemistry, Wiley/VCH Verlag, New York/Weinheim, 1999, p. 1612.
[31] V. Quéneau, S.C. Sevov, Angew. Chem. Int. Ed. Engl. 36 (1997) 1754.
[32] H.G. von Schnering, M. Baitinger, U. Bolle, W. Carrillo-Cabrera, J. Curda, Y. Grin, F. Heinemann, J. Llanos, K. Peters, A. Schmeding, M. Somer, Z. Anorg. Allg. Chem. 623 (1997) 1037.
[33] V. Quéneau, E. Todorov, S.C. Sevov, J. Am. Chem. Soc. 120 (1998) 3263.
[34] H.G. von Schnering, M. Somer, M. Kaupp, W. Carrillo-Cabrera, M. Baitinger, A. Schmeding, Y. Grin, Angew. Chem. Int. Ed. Engl. 37 (1998) 2359.
[35] T.F. Fässler, R. Hoffmann, Chimia 52 (1998) 158.
[36] C. Downie, Z. Tang, A.M. Guloy, Angew. Chem. Int. Ed. Engl. 39 (2000) 338.
[37] L. Xu, S.C. Sevov, J. Am. Chem. Soc. 121 (1999) 9245.
[38] R. Schäfer, W. Klemm, Z. Anorg. Allg. Chem. 312 (1961) 214.
[39] D. Kummer, L. Diehl, Angew. Chem. Int. Ed. Engl. 9 (1970) 895.
[40] T.F. Fässler, R. Hoffmann, Angew. Chem. Int. Ed. Engl. 38 (1999) 543.
[41] B.S. Pons, D.J. Santure, R.C. Taylor, R.W. Rudolph, Electrochim. Acta 26 (1981) 365.
[42] C.J. Warren, R.C. Haushalter, A.B. Bocarsly, J. Alloys Comp. 229 (1995) 175.
[43] T.F. Fässler, M. Hunziker, M. Spahr, H. Lueken, Z. Anorg. Allg. Chem. 626 (2000) 692.
[44] E. Zintl, Angew. Chem. 52 (1939) 1.
[45] W. Klemm, Proc. Chem. Soc. London (1959) 329.
[46] V. Quéneau, S.C. Sevov, Inorg. Chem. 37 (1998) 1358.
[47] T.F. Fässler, S. Hoffmann, Z. Kristallogr. 11 (1999) 722.
[48] M. Somer, W. Carrillo-Cabrera, E.M. Peters, K. Peters, H.G. von Schnering, Z. Anorg. Allg. Chem. 624 (1998) 1915.
[49] T.F. Fässler, U. Schütz, Inorg. Chem. 38 (1999) 1866.
[50] N. Korber, Phosphorus Sulfur 125 (1997) 339.
[51] K. Wade, Adv. Inorg. Chem. Radiochem. 18 (1976) 1.
[52] R.W. Rudolph, W.L. Wilson, F. Parker, R.C. Taylor, D.C. Young, J. Am. Chem. Soc. 100 (1978) 4629.
[53] R.W. Rudolph, W.L. Wilson, R.C. Taylor, J. Am. Chem. Soc. 103 (1981) 2480.
[54] E.L. Mutterties, E.L. Hoel, C.G. Salentine, M.F. Hawthorne, Inorg. Chem. 14 (1975) 950.
[55] M.E. O'Neill, K. Wade, Polyhedron 2 (1983) 963.
[56] L.J. Guggenberger, E.L. Muetterties, J. Am. Chem. Soc. 98 (1976) 7221.
[57] L.L. Lohr, Inorg. Chem. 20 (1981) 4229.
[58] J. Campbell, D.A. Dixon, H.P.A. Mercier, G.J. Schrobilgen, Inorg. Chem. 34 (1995) 5798.
[59] T.F. Fässler, M. Hunziker, Z. Anorg. Allg. Chem. 622 (1996) 837.
[60] T.F. Fässler, Habilitationsschrift, ETH Zürich, 1997.
[61] L.J. Guggenberger, Inorg. Chem. 7 (1968) 2260.
[62] R. Hoffmann, Dissertation, ETH Zürich, 2000.
[63] H. Mercier, C. Belin, J. Chim. Phys. 86 (1989) 1643.
[64] R.M. Friedman, J.D. Corbett, Inorg. Chem. 12 (1973) 1134.
[65] A. Hershaft, J.D. Corbett, Inorg. Chem. 2 (1963) 979.
[66] M.B. Hursthouse, J. Kane, A.G. Massey, Nature 228 (1970) 659.
[67] W. Hönle, Y. Grin, A. Burkhardt, U. Wedig, M. Schultheiss, H.G. von Schnering, J. Sol. State Chem. 133 (1997) 59.
[68] J. Campbell, G.J. Schrobilgen, Inorg. Chem. 36 (1997) 4078.
[69] M. Somer, W. Carrillo-Cabrera, E.M. Peters, K. Peters, M. Kaupp, H.G. von Schnering, Z. Anorg. Allg. Chem. 625 (1999) 37.
[70] T.P. Martin, Angew. Chem. Int. Ed. Engl. 25 (1986) 197.
[71] D. Schild, R. Pflaum, K. Sattler, E. Recknagel, J. Phys. Chem. 91 (1987) 2649.
[72] A. Hartmann, K.G. Weil, High Temp. Sci. 27 (1990) 31.
[73] T.F. Fässler, H.-J. Muhr, M. Hunziker, Inorg. Chem. Eur. J. (1998) 1433.
[74] B.W. Eichhorn, R.C. Haushalter, J. Am. Chem. Soc. 110 (1988) 870.

[75] B.W. Eichhorn, R.C. Haushalter, J. Chem. Soc. Chem. Commun. (1990) 937.
[76] T.F. Fässler, U. Schütz, J. Organomet. Chem. 541 (1997) 269.
[77] D.R. Gardner, J.C. Fettinger, B.W. Eichhorn, Angew. Chem. Int. Ed. Engl. 35 (1999) 2852.
[78] R.M. Fleming, A.P. Ramirez, M.J. Rosseinsky, D.W. Murphy, R.C. Haddon, S.M. Zahurak, A.V. Makhija, Nature 352 (1991) 787.
[79] S.S. Eaton, A. Kee, R. Konda, G.R. Eaton, P.C. Trulove, R.T. Carlin, J. Phys. Chem. 100 (1996) 6910.
[80] T.F. Fässler, A. Spiekermann, M. Spahr, R. Nesper, Angew. Chem. Int. Ed. Engl. 36 (1997) 486.
[81] T.F. Fässler, R. Hoffmann, S. Hoffmann, M. Wörle, Angew. Chem. Int. Ed. Engl. 39 (2000) 2091.
[82] P.W. Stephens, G. Bortel, G. Faigel, M. Tegze, A. Jánossy, S. Pekker, G. Oszlanyi, L. Forró, Nature 370 (1994) 636.
[83] E. Todorov, S.C. Sevov, Inorg. Chem. 37 (1998) 3889.
[84] T.F. Fässler, R. Hoffmann, J. Chem. Soc. Dalton Trans. (1999) 3339.
[85] M. Weidenbruch, Angew. Chem. Int. Ed. Engl. 32 (1993) 545.
[86] P.A. Edwards, J.D. Corbett, Inorg. Chem. 16 (1977) 903.
[87] P. Kirchner, G. Huttner, K. Heinze, G. Renner, Angew. Chem. Int. Ed. Engl. 37 (1998) 1664.
[88] B. Schiemenz, G. Huttner, Angew. Chem. Int. Ed. Engl. 23 (1993) 297.
[89] L.J. Guggenberger, Inorg. Chem. 8 (1969) 2771.
[90] H. von Benda, A. Simon, W. Bauhofer, Z. Anorg. Allg. Chem. (1978) 53.
[91] T.F. Fässler, M. Hunziker, Inorg. Chem. 33 (1994) 5380.
[92] C. Hoch, C. Röhr, P. Zönnchen, 18th European Crystallographic Meeting, Praha, 1998, 388pp.
[93] T.F. Fässler, R. Hoffmann, Z. Kristallogr. NCS 215 (2000) 139.
[94] J.D. Corbett, P.A. Edwards, J. Am. Chem. Soc. 99 (1977) 3313.
[95] R. Burns, J.D. Corbett, Inorg. Chem. 24 (1985) 1489.
[96] S.C. Critchlow, J.D. Corbett, J. Am. Chem. Soc. 105 (1983) 5715.
[97] R. Hauptmann, R. Hoffmann, T.F. Fässler, in preparation.
[98] V. Quéneau, S.C. Sevov, Inorg. Chem. 37 (1998) 1358.
[99] T.F. Fässler, M. Hunziker, Inorg. Chem. 33 (1994) 5380.